AGU PUBLICATIONS

JGR

Journal of Geophysical Research: Atmospheres

RESEARCH ARTICLE
10.1002/2013JD021401

Key Points:
- Flash and stroke detection efficiencies of the NLDN are 94% and 75%, respectively
- Median location error of the NLDN is 334 m
- Median value of absolute peak current estimation error is 14%

Supporting Information:
- Readme
- Table S1
- Figure S1

Correspondence to:
V. A. Rakov,
rakov@ece.ufl.edu

Citation:
Mallick, S., et al. (2014), Performance characteristics of the NLDN for return strokes and pulses superimposed on steady currents, based on rocket-triggered lightning data acquired in Florida in 2004–2012, *J. Geophys. Res. Atmos.*, *119*, 3825–3856, doi:10.1002/2013JD021401.

Received 21 DEC 2013
Accepted 17 MAR 2014
Accepted article online 18 MAR 2014
Published online 9 APR 2014

Performance characteristics of the NLDN for return strokes and pulses superimposed on steady currents, based on rocket-triggered lightning data acquired in Florida in 2004–2012

S. Mallick[1], V. A. Rakov[1], J. D. Hill[1,2], T. Ngin[1], W. R. Gamerota[1], J. T. Pilkey[1], C. J. Biagi[1,3], D. M. Jordan[1], M. A. Uman[1], J. A. Cramer[4], and A. Nag[5]

[1]Department of Electrical and Computer Engineering, University of Florida, Gainesville, Florida, USA, [2]Stinger Ghaffarian Technologies, Kennedy Space Center, Florida, USA, [3]Lightning Technologies, an NTS Company, Pittsfield, Massachusetts, USA, [4]Vaisala Inc., Tucson, Arizona, USA, [5]Vaisala Inc., Louisville, Colorado, USA

Abstract We present a detailed evaluation of performance characteristics of the U.S. National Lightning Detection Network (NLDN) using, as ground truth, Florida rocket-triggered lightning data acquired in 2004–2012. The overall data set includes 78 flashes containing both the initial stage and leader/return-stroke sequences and 2 flashes composed of the initial stage only. In these 80 flashes, there are a total of 326 return strokes (directly measured channel-base currents are available for 290 of them) and 173 kiloampere-scale (≥1 kA) superimposed pulses, including 58 initial continuous current pulses and 115 M components. All these events transported negative charge to the ground. The NLDN detected 245 return strokes and 9 superimposed pulses. The resultant NLDN flash detection efficiency is 94%, return-stroke detection efficiency is 75%, and detection efficiency for superimposed pulses is 5% for peak currents ≥1 kA and 32% for peak currents ≥5 kA. For return strokes, the median location error is 334 m and the median value of absolute peak current estimation error is 14%. The percentage of misclassified events is 4%, all of them being return strokes. The median value of absolute event-time mismatch (the difference in times at which the event is reported to occur by the NLDN and recorded at the lightning triggering facility) for return strokes is 2.8 μs. For two out of the nine superimposed pulses detected by the NLDN, we found optical evidence of a reilluminated branch (recoil leader) coming in contact with the existing grounded channel at an altitude of a few hundred meters above ground.

1. Introduction

Since 1989, the U.S. National Lightning Detection Network (NLDN), currently operated by Vaisala Inc., has been providing lightning data for the contiguous United States. Upgrades to the network were made in 1994–1995 [*Cummins et al.*, 1998], 2003–2004 [*Cummins and Murphy*, 2009], 2010–2012 [*Nag et al.*, 2013a], and in April–August 2013 [*Nag et al.*, 2013b]. The 2010–2012 upgrade is discussed in detail in section 2. Figure 1 shows the locations of 17 NLDN sensors in and around the Florida region as of 2009.

Jerauld et al. [2005] and *Nag et al.* [2011] used rocket-triggered lightning data, acquired at International Center for Lightning Research and Testing at Camp Blanding, Florida, (referred to in the following as Camp Blanding) to evaluate the performance of the NLDN for the periods of 2001–2003 and 2004–2009, respectively. In 2001–2003, 37 flashes containing 159 (158 negative and 1 positive) return strokes were triggered at Camp Blanding. The resultant flash and stroke detection efficiencies were 84% and 60%, respectively. The median location error was 600 m. The median value of absolute peak current estimation error was 20%. The sample size for evaluation of errors in peak current estimates was 70. In 2004–2009, 37 flashes containing 139 negative return strokes were triggered at Camp Blanding. The flash and stroke detection efficiencies were 92% and 76%, respectively, and the median location error was 308 m. The median value of absolute peak current estimation error was 13%. The sample size for evaluation of errors in peak current estimates was 96. *Nag et al.* [2011] interpreted their 2004–2009 results as an improvement in performance characteristics of the NLDN due to its upgrade completed in 2004.

Triggered lightning is typically composed of an initial stage (upward positive leader and initial continuous current) and one or more downward leader/upward return-stroke sequences. The results of *Jerauld et al.* [2005] and *Nag et al.* [2011], based on using triggered-lightning data as the ground truth, are applicable only

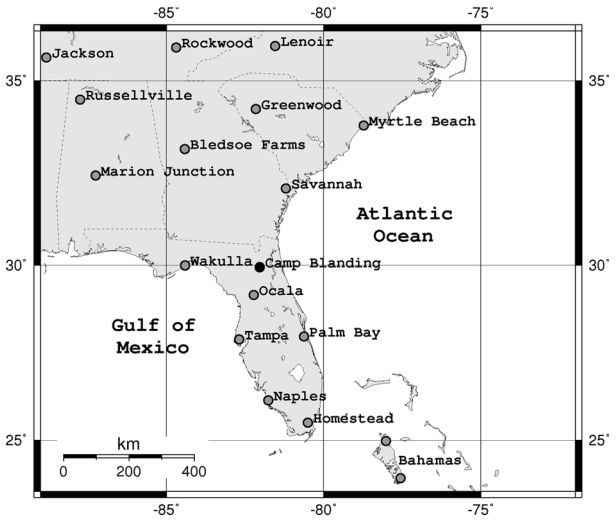

Figure 1. Map showing the locations of 17 NLDN sensors (gray circles) in and around Florida. The approximate location of Camp Blanding (black circle) is also shown. The map applies to all years considered in this paper (2004–2012), except for the two sensors in the Bahamas that were installed in 2006.

to negative subsequent return strokes in natural downward lightning (or flashes without first strokes in the case of flash detection efficiency). This is because in triggered-lightning flashes the first stroke of a natural flash, involving a descending stepped leader, is in effect replaced by the initial-stage process with very different parameters, while subsequent strokes in triggered and natural flashes are similar [e.g., *Rakov and Uman*, 2003].

Besides return strokes (or just strokes), the NLDN is capable of recording sufficiently large pulses superimposed on steady currents occurring during the initial stage of rocket-triggered or object-initiated lightning (usually referred to as initial continuous current pulses), as well as on similar currents following some return-stroke pulses in both downward and upward flashes (M components). The NLDN performance characteristics for such superimposed pulses (SIPs) are presently unknown.

Fisher et al. [1993] found that triggered-lightning return strokes were invariably preceded by a time interval without measurable current flowing to ground (the minimum detectable current level was <2 A), implying that an essentially complete cutoff in channel current is a prerequisite for the formation of a subsequent leader/return-stroke sequence. This finding is consistent with the observations of *McCann* [1944] and *Berger* [1967], who reported that the current between strokes fell below their systems' minimum detectable levels of 0.1 A and 1 A, respectively. The virtual absence of steady current prior to the current pulse measured at the strike point is thought to be indicative of the leader/return-stroke mode of charge transfer to ground [*Rakov et al.*, 2001]. On the other hand, "classical" M components and some of the initial continuous current (ICC) pulses develop along relatively long grounded channel sections (a kilometer or more in length) that carry steady currents, typically in the tens to hundreds of amperes range. The corresponding mode of charge transfer to ground is referred to as the M component mode. In the presence of relatively low-level upward branches, the so-called mixed mode [*Zhou et al.*, 2011] of charge transfer to ground can occur, in which a dart leader/return-stroke sequence occurs in one decayed branch, while another grounded branch is carrying a steady current. As a result, a sharp pulse characteristic of return strokes, superimposed on a steady current, which is a feature of M components, can be measured at the strike object.

In this paper, rocket-triggered lightning data, acquired in 2004–2012 at Camp Blanding, are used for evaluating NLDN performance characteristics. In addition to NLDN performance characteristics for return-stroke pulses (RSs), the NLDN performance characteristics for kiloampere-scale ($\geq$1 kA) pulses superimposed on steady currents, referred to here as superimposed pulses (SIPs), are presented for the first time. As discussed earlier, the "classical" return strokes are generally preceded by essentially zero-current (below 1–2 A or less) intervals and superimposed pulses are riding either on the initial-stage current

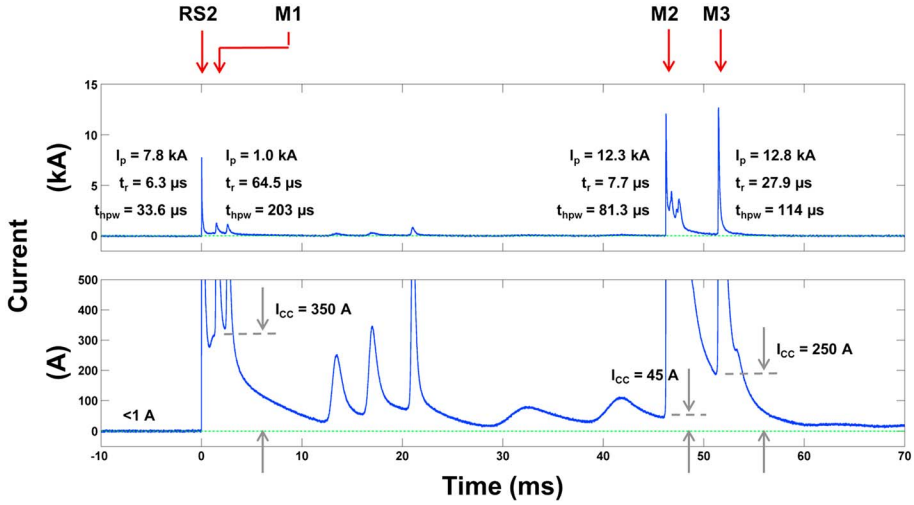

Figure 2. Channel-base current of the second return stroke (RS2) of flash UF 09-06 and its continuing current with several M components, shown on 15 kA (top) and 500 A (bottom) scales. The flash transported negative charge to ground. Three kiloampere-scale M components are labeled M1, M2, and M3, with M2 and M3 having unusually high peak currents. Steady current levels prior to RS2, M1, M2, and M3 are indicated. The NLDN detected RS2 and M3 as cloud-to-ground (CG) events and did not detect M1 and M2. I_P is the peak of current pulse relative to the preceding background level (I_{CC} in the case of M components), t_r is its 10 to 90% risetime, and t_{hpw} is its half-peak width.

(ICC pulses) or on continuing currents (M components) following return-stroke pulses. Figure 2 shows an example of return stroke followed by three kiloampere-scale pulses superimposed on continuing current, with all the processes transporting negative charge to ground. In this paper, we do not make a distinction between the mixed mode [*Zhou et al.*, 2011] and "classical" M component mode [*Rakov et al.*, 2001] of charge transfer to ground. Accordingly, any pulse preceded by a steady current ≥1 A was labeled "M component" if it followed a return stroke, and it was labeled "ICC pulse" if it occurred during the initial stage of triggered-lightning flash. In discussing our results for ICC pulses, we do consider the corresponding video and still camera records with vertical fields of view ranging from 290 m to 400 m above the rocket launcher in an attempt to identify relatively low upward branching points that are indicative of the mixed mode. NLDN performance characteristics for kiloampere-scale superimposed pulses have important implications for detectability by the NLDN of tower-initiated flashes, which often do not contain return strokes [e.g. *Rakov and Uman*, 2003, chap. 6; *Diendorfer et al.,* 2009]. Additionally, we perform a detailed analysis of NLDN-reported location error ellipses and chi-squared values corresponding to the optimum (reported) location.

2. The 2010–2012 NLDN Upgrade

The 2010–2012 upgrade is described in more detail here [see also *Nag et al.*, 2013a] because it apparently influenced the NLDN performance characteristics presented in this paper. There were two distinct steps in the transition between early 2010 and 2012.

The first step, implemented in 2010, was the introduction of propagation corrections (to account for finite ground conductivity and terrain over which the lightning electromagnetic signals propagate) for the IMPACT (Improved Accuracy Through Combined Technology) sensors in the NLDN. This reduced the errors in the arrival time measurement by a factor of 2, with the expected median location error less than 250 m [*Cummins et al.,* 2010] in the interior of the network. On 28 December 2010, the minimum reportable length of the 50% error ellipse semimajor axis (SMA) was reduced from 400 m to 200 m, to reflect the expected improvement in location accuracy.

The second step involved a gradual replacement of all analog IMPACT sensors with the fully digital LS7001 sensors [*Cummins et al.*, 2012]. The deployment of LS7001 sensors began in the spring of 2011, and about 80% of the IMPACT sensors in the NLDN had been replaced by 11 August 2011. The sensors in and around the

Table 1. Summary of Flashes Triggered at Camp Blanding During 2004–2012 Along With the NLDN Flash and Return-Stroke Detection Efficiencies

Time Period	Number of Flashes with Return Strokes	Number of NLDN-Detected Flashes	NLDN Flash Detection Efficiency	Number of Strokes	Number of NLDN-Detected Strokes	NLDN Stroke Detection Efficiency
2004–2012[a,b]	78	73	94%	326	245	75%
2004–2009[a] [*Nag et al.*, 2011]	37	34	92%	139	105	76%
2001–2003 [*Jerauld et al.*, 2005]	37	31	84%	159	95	60%

[a]There was no lightning triggered in 2006 at Camp Blanding.
[b]There were no flashes with return strokes, in which at least one superimposed pulse was detected and none of the return strokes were detected by the NLDN; that is, there were no flashes with return strokes that were detected via SIPs.

Florida region were completely replaced by early May 2011. In December 2011, it became clear that the propagation corrections, introduced in the first step and developed for the IMPACT sensors, were not well suited for LS7001 sensors. The problem was rectified in February 2012 by eliminating the propagation corrections (applied at the central processor) and enabling the sensor-based timing onset corrections described by *Honma et al.* [2013].

Between April and August 2013, the LS7001 sensors were upgraded to LS7002 to improve detection of lower amplitude lightning events (primarily cloud pulses). This required a change to the analog signal conditioning and digital signal processing in the sensor's embedded software [*Nag et al.*, 2013b]. Additionally, small refinements to the sensor-based timing onset corrections for better performance under low signal-to-noise ratio conditions were implemented. Our results are concerned with the NLDN performance characteristics prior to the 2013 upgrade.

3. Data and Methodology

In 2004–2012, a total of 223 rockets trailing grounded wires were launched at Camp Blanding, which resulted in 110 triggered-lightning flashes, with 78 flashes having leader/return-stroke sequences. Note that no triggering rockets were launched in 2006. In the present study, we analyzed all 78 flashes having leader/return-stroke sequences and 2 flashes composed of the initial stage only. The overall data set consists of 326 negative return strokes and 173 kiloampere-scale (≥1 kA) superimposed pulses (58 ICC pulses and 115 M components). All peak currents are given as positive values throughout the paper. The average number of strokes per flash was 4.2 (326/78). Table 1 gives a summary of flashes and strokes recorded at Camp Blanding during 2004–2012, and Table 2 gives a similar summary of kiloampere-scale superimposed pulses recorded at Camp Blanding during the same time period. Data acquired prior to 2004 were not included because of the major NLDN upgrade that was in progress in 2003–2004. Only 2 flashes (one from 2009 and one from 2011) without return strokes out of 32 were included in this study, because these two flashes contained well-documented ICC pulses with unusually high peaks, relatively short 10 to 90% risetimes, and relatively small half-peak widths. The remaining 30 flashes without return strokes were not included, because information on ICC pulses in these flashes is not readily available. Hence, our analysis of ICC pulses is biased toward flashes with return strokes.

Three rocket launchers (a ground launcher, a tower launcher, and a mobile launcher) were used in 2004–2012, and the positions of the launchers are known to within a few meters. There were two flashes in which the

Table 2. Summary of Kiloampere-Scale Superimposed Pulses (ICC Pulses and M Components) Recorded at Camp Blanding During 2004–2012 Along With the NLDN Detection Efficiencies for Two Selection Criteria (≥1 kA and ≥5 kA)

	ICC Pulses			M Components			SIPs (ICC Pulses + M Components)		
Selection Criterion	Recorded at Camp Blanding	Detected by the NLDN	NLDN Detection Efficiency	Recorded at Camp Blanding	Detected by the NLDN	NLDN Detection Efficiency	Recorded at Camp Blanding	Detected by the NLDN	NLDN Detection Efficiency
≥1 kA	58	7	12%	115	2	2%	173	9	5%
≥5 kA	13	6	46%	12	2	17%	25	8	32%

lightning channel did not terminate on the instrumented facility, and in these two cases, the location of the ground attachment point was determined, also with an uncertainty of a few meters, from optical still images and video records. The channel-base current was measured by resistive shunts with a bandwidth of 0 to at least 3 MHz (typically 8 MHz). There were multiple channel-base current measurements that were labeled as high (of the order of tens of kiloamperes), low (of the order of kiloamperes), very low (of the order of hundreds of amperes), and extra low (of the order of milliamperes). The number of channel-base current measurements and exact current ranges varied from year to year. Fiber-optic links were used to transmit signals from the sensors to digitizing oscilloscopes. Two oscilloscopes were used to record current waveforms. A 12-bit oscilloscope, with record length in the range of 0.8–2 s, was used to record overall current waveform for the entire flash. The sampling rate of the 12-bit oscilloscope was 2, 10, or 100 MHz with the signals being low-pass filtered (−3 dB at 500 kHz, 3 MHz, and 20 MHz, respectively) before digitization. An 8-bit oscilloscope, with record length in the range of 1–5 ms and running in segmented mode (multiple triggers per flash), was used to record individual pulses (return strokes, ICC pulses, and M components). The sampling rate of the 8-bit oscilloscope was 20, 100, or 250 MHz with the signals being low-pass filtered (−3 dB at 5 MHz, 20 MHz, and 20 MHz, respectively) before digitization. The oscilloscopes triggered when the channel-base current exceeded a preset threshold or when the two optical detectors, viewing the triggering site from opposite corners, simultaneously detected luminosity from the lightning channel. The trigger threshold was some kiloamperes. Note that the current trigger threshold does not cause a bias because of the availability of entire-flash current records.

For 2004–2011 data, whenever possible, peak currents were measured in 8-bit oscilloscope records which have a smaller sampling interval (50 ns, 10 ns, or 4 ns); otherwise, peak currents were measured in 12-bit oscilloscope records. For 2012 data, peak currents were measured in the 12-bit oscilloscope records with sampling rate of 100 MHz, with the exception of three strokes for which 12-bit records were not available and their peak currents were measured in 8-bit oscilloscope records. The recorded waveforms were smoothed before analysis using a five-point moving average technique to reduce noise. The directly measured current peaks may contain errors up to 10% or so [*Jerauld et al.*, 2005], but for the purpose of this study they are assumed to be the absolute ground truth.

In the previous studies [*Jerauld et al.*, 2005; *Nag et al.*, 2011], no distinction was made between return strokes and superimposed pulses. In the present study, the steady current level immediately prior to the pulse onset was examined in current waveforms to categorize the pulse either as a return stroke or a superimposed pulse. Any pulse preceded by steady current ≥1 A was considered a superimposed pulse. In case of unavailability of current records (for 36 strokes due to instrumentation malfunctioning or lightning channel not terminating on the instrumented facility), channel luminosity in high-speed video records was used to differentiate between return strokes and superimposed pulses (no detectable luminosity prior to abrupt channel illumination was assumed to be indicative of return stroke). For superimposed pulses, the peak value of the pulse was found by subtracting the steady current level immediately prior to the pulse from the peak value measured with respect to the zero level.

The following NLDN performance characteristics were determined: (a) flash and return-stroke detection efficiencies, (b) superimposed pulse detection efficiency, (c) percentage of misclassified events, (d) location accuracy, and (e) peak current estimation error. Evaluation of the NLDN performance characteristics based on independent, ground truth observations (particularly errors in locations and peak current estimates) can be viewed as a kind of calibration of the network. Camp Blanding and NLDN events were correlated using GPS time stamps. The detection efficiency values were computed as the ratios of the numbers of NLDN-detected events and all triggered-lightning events recorded at Camp Blanding. Since all the triggered-lightning strokes examined here were negative strokes to ground (−CG events), the percentage of misclassified events is the number of NLDN-detected events that were reported as not −CGs, expressed in percent of the total number of NLDN-detected events. For a given event, the distance between the location of rocket launcher or the lightning ground attachment point (used as ground truth) and the location reported by the NLDN is defined as the location error (Δr). The north-south and east-west components of the location error were also computed. The errors in NLDN-reported peak currents were computed using the equation $\Delta I = I_{NLDN} - I_{CB}$, where I_{NLDN} is the NLDN-reported peak current and I_{CB} is the peak value of current waveform directly measured at Camp Blanding. The current error is expressed in percent of I_{CB}.

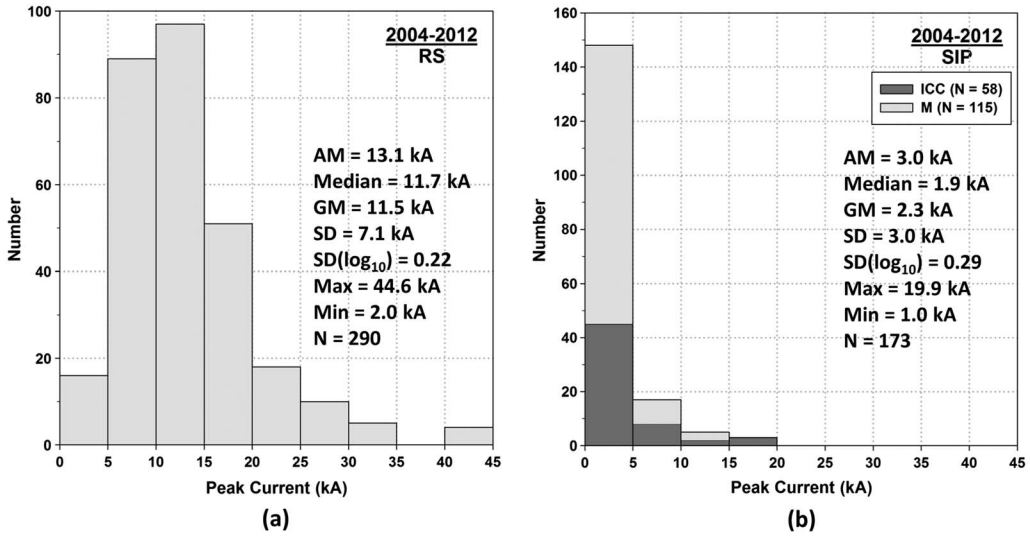

Figure 3. Histograms of peak currents directly measured at Camp Blanding in 2004–2012 for (a) return strokes and (b) kiloampere-scale superimposed pulses, both detected and not detected by the NLDN. Statistics given are the arithmetic mean (AM), median, geometric mean (GM), standard deviation (SD), standard deviation of the $\log_{10}$ of the parameter (SD($\log_{10}$I)), maximum value (Max), and minimum value (Min). *N* is the sample size.

Additionally, we examined the event-time mismatch which was computed as $\Delta t = t_{NLDN} - t_{CB}$, where t_{NLDN} is the NLDN-reported time for an event and t_{CB} is the precise (within 1 μs) GPS time of the event recorded at Camp Blanding. The event time reported by the NLDN is one of the outputs of the NLDN locating algorithm and corresponds to the beginning of electromagnetic field pulse generated by that event, whereas the GPS timestamp recorded at Camp Blanding corresponds to the time when the lightning current exceeded the preset threshold of some kiloamperes or the luminosity of the lightning channel became strong enough to trigger the two optical detectors viewing the research site from its opposite corners.

Of the 326 strokes in 78 flashes recorded at Camp Blanding in 2004–2012, directly measured currents were available for 290 strokes in 73 flashes. The NLDN detected 245 strokes out of the total of 326 strokes (of these 245 strokes, directly measured currents were available for 222). Figure 3 shows the peak current histograms for all return strokes and superimposed pulses recorded at Camp Blanding during 2004–2012 (regardless of whether they were detected by the NLDN). For return-stroke peak currents, the geometric mean (GM) is 11.5 kA, median is 11.7 kA, maximum is 44.6 kA, and minimum is 2.0 kA. For peak currents

Table 3. Arithmetic Mean, Minimum, and Maximum Number of Reporting NLDN Sensors for Different Peak Current Ranges for Both Return Strokes and Kiloampere-Scale Superimposed Pulses

Range (kA) Peak Current	Number of Reporting Sensors[a]			
	Arithmetic Mean	Minimum	Maximum	Sample Size
0–5	-	4	4	1 (0)
5–10	4 (4)	2 (2)	6 (6)	53 (50)
10–15	5 (5)	3 (3)	10 (10)	89 (87)
15–20	7 (7)	2 (3)	11 (11)	52 (49)
20–25	8 (8)	5 (5)	11 (11)	17 (17)
25–30	8 (8)	5 (5)	11 (11)	10 (10)
30–35	9 (9)	4 (4)	11 (11)	5 (5)
35–40	-	-	-	0 (0)
40–45	12 (12)	9 (9)	14 (14)	4 (4)
0–45	6 (6)	2 (2)	14 (14)	231 (222)

[a]Numbers in the parentheses are for return strokes only.

Table 4. Summary of Kiloampere-Scale Superimposed Pulses Detected by the NLDN During 2004–2012[a]

Flash ID	SIP ID	I_{CB} (kA)	I_{CC} (A)	I_{NLDN} (kA)	SMA (km)	ΔI (%)	Δr (km)	Δt (μs)	t_r (μs)	t_{hpw} (μs)	Evidence of Upward Branching
UF 08-08	ICC1	6.5	<20	5.8	1.1	−11	0.5	N/A	3.9	25.7	None within 400 m
UF 09-06	M3 (RS2)	12.8	250	7.5	0.6	−41	0.4	N/A	27.9	114	None within 400 m
UF 09-42	ICC1	15.2	70	15.2	7.6	0	0.8	N/A	9	65.9	None within 400 m
UF 10-23	ICC2	16.0	90	8.8	2.6	−45	1.3	N/A	11.5	63.5	329 m above launcher
UF 10-24	ICC1	11.5	2	11.8	0.4	3	0.4	0	1	29.1	None within 340 m
UF 11-08	ICC4	4.9	<100	6.3	0.5	29	0	0	1.8	27.1	None within 390 m
UF 11-15	ICC3	19.9	100	16	0.2	−20	0.5	−3	10.9	140	None within 290 m
UF 11-35	M1 (RS2)	8.9	3	6.4	5.3	−28	4.7	14	1.3	28.0	None within 390 m
UF 12-48	ICC2	9.0	10	8.1	2.8	−10	0.9	−3	7.1	63.7	330 m above launcher
	AM	11.6		9.5	2.3	−14	1.1	1.6	8.3	61.8	
	Median	11.5		8.1	1.1	−11	0.5	0	7.1	63.5	
	N	9		9	9	9	9	5	9	9	

[a]For M components, the preceding return-stroke ID is given in the parentheses in the SIP ID column. I_{CC} is the preceding steady current level. SMA is the semimajor axis length of error ellipse reported by the NLDN. The t_r is the 10 to 90% risetime, and t_{hpw} is the half-peak width. N/A in the Δt column indicates that the value is not available due to unavailability of precise GPS timestamp. All the superimposed pulses were detected as cloud-to-ground (CG) events. AM is the arithmetic mean, and *N* is the sample size.

of superimposed pulses, the GM is 2.3 kA, median is 1.9 kA, maximum is 19.9 kA, and minimum is 1.0 kA (the assumed cutoff level in this study). The average number of reporting sensors for different peak current ranges is given in Table 3.

Precise (within 1 μs) GPS times (needed for the event-time mismatch analysis; see section 4.6), recorded at Camp Blanding, were available for 134 (129 return strokes, 4 ICC pulses, and 1 M component) out of 254 events detected by the NLDN during 2004–2012.

It is worth noting that the data for the period of 2004–2009 (the data used by *Nag et al.* [2011]) have been reexamined (to better differentiate between return strokes and superimposed pulses) and reprocessed in this study. As a result, there are minor differences in some values given here and those previously reported by *Nag et al.* [2011]. For example, the maximum current estimation error for 2004–2012 corresponds to a return stroke in a flash triggered in 2008. The value of this error given in section 4.5 of the present paper is 127% versus 129% reported by *Nag et al.* [2011]. None of the results of the previous study is materially affected by the data reprocessing.

Table 5. Summary of Return Strokes Misclassified by the NLDN as Cloud (IC) Events During 2004–2012[a]

Flash ID	Stroke ID	I_{CB} (kA)	I_0 (A)	I_{NLDN} (kA)	SMA (km)	ΔI (%)	Δr (km)	Δt (μs)	t_r (μs)	t_{hpw} (μs)
UF 08-02	RS4	13.9	20	14	0.4	1.0	0.4	N/A	0.5	13.6
UF 09-11	RS1	N/A	-	20	0.4	-	0.3	2	-	-
UF 09-11	RS3	N/A	-	6.4	0.6	-	0.7	N/A	-	-
UF 09-13	RS3	N/A	-	14.8	0.4	-	0.3	N/A	-	-
UF 09-22	RS4	6.6	0.1	5.3	3.2	−20	2.4	N/A	0.6	11.7
UF 09-25	RS1	6.2	0.1	5.3	3.0	−15	0.3	N/A	2.7	26.4
UF 10-18	RS1	N/A	-	6.2	3.6	-	0.8	N/A	-	-
UF 11-28	RS1	19.2	0.01	18.7	0.2	−3.0	0.3	−1	0.3	37.6
UF 12-04	RS1	N/A	-	10.7	0.2	-	0.2	−3	-	-
	AM	11.5		11.3	1.3	−9	0.6	−0.7	1.0	22.3
	Median	10.3		10.7	0.4	−9	0.3	−1	0.55	20
	N	4		9	9	4	9	3	4	4

[a]I_0 is the lower current measurement limit. SMA is the semimajor axis length of error ellipse reported by the NLDN. The t_r is the 10 to 90% risetime, and t_{hpw} is the half-peak width. N/A in the I_{CB} column indicates that no current was recorded owing to instrument malfunction or lightning channel not attaching to instrumented facility. When current waveforms were not recorded, channel luminosity in high-speed video records was used to differentiate between return strokes and superimposed pulses. N/A in the Δt column indicates that the value is not available due to unavailability of precise GPS timestamp. AM is the arithmetic mean, and *N* is the sample size.

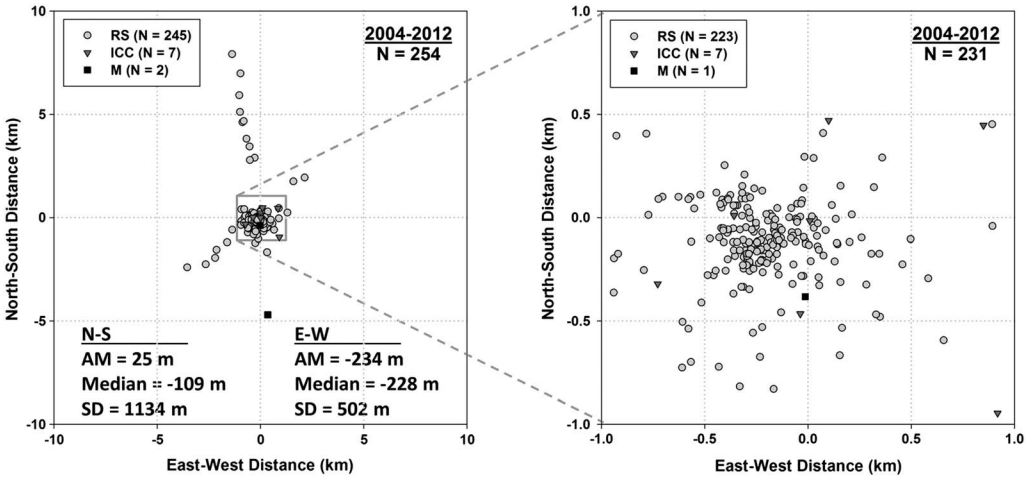

Figure 4. Plot of NLDN-reported locations for 254 events in 80 flashes triggered during 2004–2012 at Camp Blanding. Different plot symbols are used for return strokes (RS), ICC pulses (ICC), and M components (M). The origin of coordinates corresponds to the actual event location. Statistics given (for return strokes, ICC pulses, and M components combined, $N = 254$) are arithmetic mean (AM), median, and standard deviation (SD), for each location error component.

4. Results

4.1. Flash and Return-Stroke Detection Efficiencies

Detection efficiencies for flashes and return strokes (SIPs are considered separately in section 4.2) from this study and previous studies are summarized in Table 1. In 2004–2012, the NLDN flash detection efficiency was 94% and the stroke detection efficiency was 75%, both values being consistent with those reported for 2004–2009 by *Nag et al.* [2011]. Note that in all detected flashes with return strokes at least one return stroke was detected; that is, none of those flashes was detected solely via a superimposed pulse (or pulses), so that the flash detection efficiency value for 2004–2012 is directly comparable to its counterparts from earlier studies, when SIPs were generally not considered.

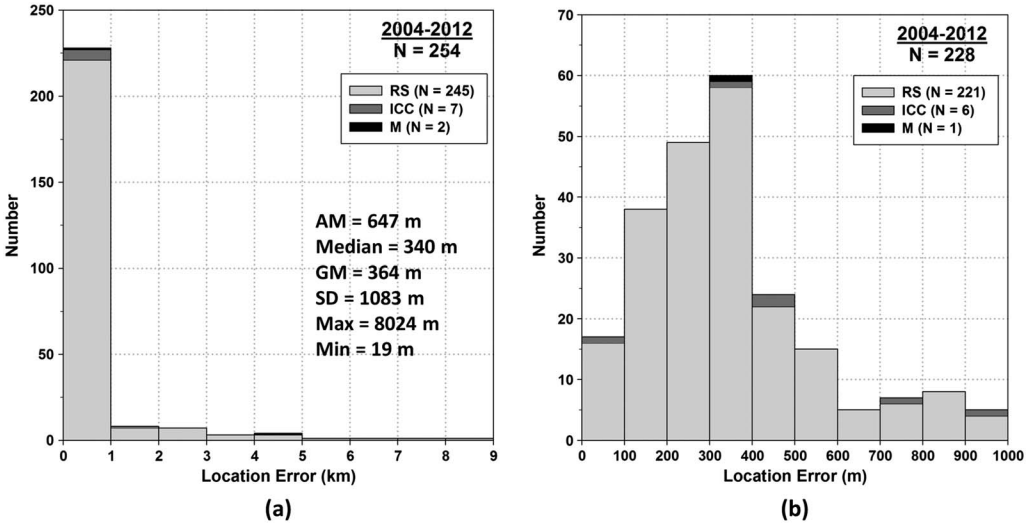

Figure 5. Histograms of NLDN location errors for (a) all 254 events in 80 flashes triggered in 2004–2012 and (b) 228 events with location errors ≤1 km. Different types of shading are used for return strokes (RS), ICC pulses (ICC), and M components (M). Statistics given (for return strokes, ICC pulses, and M components combined, $N = 254$) are the arithmetic mean (AM), median, geometric mean (GM), standard deviation (SD), maximum value (Max), and minimum value (Min).

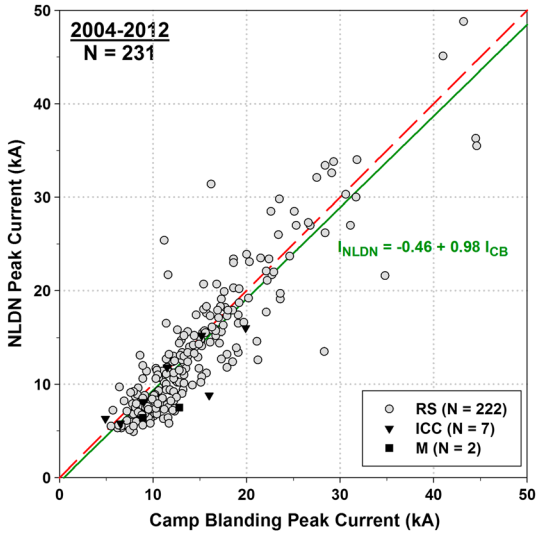

Figure 6. NLDN-reported peak current versus peak current directly measured at Camp Blanding for 231 events in 80 flashes triggered in 2004–2012. Different plot symbols are used for return strokes (RS), ICC pulses (ICC), and M components (M). The solid line, $I_{NLDN} = -0.46 + 0.98 \times I_{CB}$, is the best (least squares) fit to the data (for return strokes, ICC pulses, and M components combined, $N = 231$), while the broken line represents the ideal situation when $I_{NLDN} = I_{CB}$. For the 222 return strokes, the regression equation is slightly different: $I_{NLDN} = -0.43 + 0.98 \times I_{CB}$.

4.2. Superimposed Pulse Detection Efficiency

In 2004–2012, the NLDN detected 9 out of 173 superimposed pulses, of which 7 were ICC pulses and 2 were M components. The NLDN detection efficiency for superimposed pulses with peaks ≥1 kA was 5%, and that for pulses with peaks ≥5 kA was 32% (see Table 2). The detection efficiency for ICC pulses is considerably higher than that for M components. Geometric mean values of peak currents for ICC pulses and M components are 2.7 kA and 2.1 kA, respectively, which apparently explains the higher detection efficiency for ICC pulses.

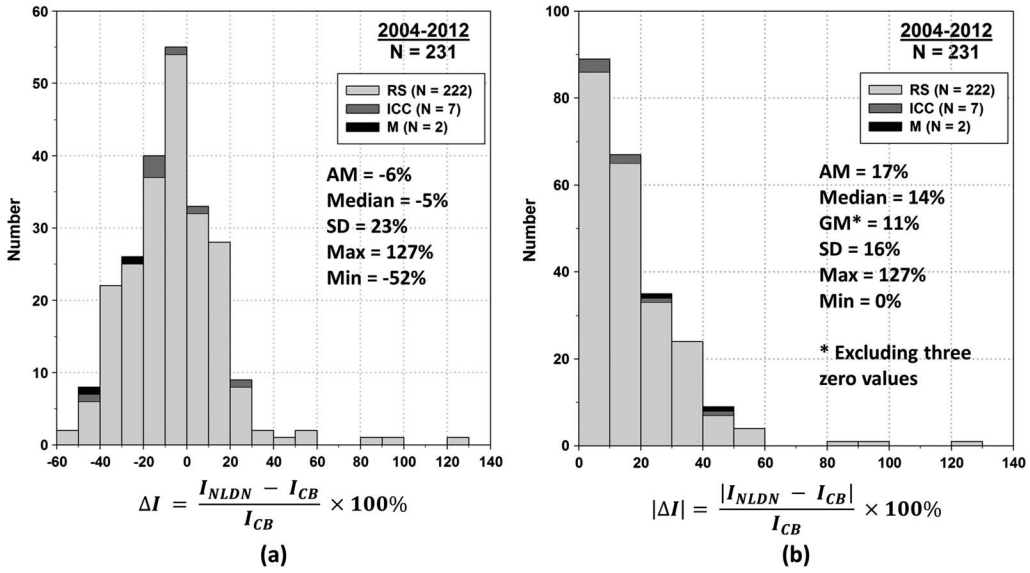

Figure 7. Histograms of (a) signed and (b) absolute NLDN peak current estimation errors, given as a percentage of the directly measured Camp Blanding current ($\Delta I\% = 100\Delta I/I_{CB}$, where $\Delta I = I_{NLDN} - I_{CB}$) for 231 events in 80 flashes triggered in 2004–2012. Different types of shading are used for return strokes (RS), ICC pulses (ICC), and M components (M). Statistics given (for return strokes, ICC pulses, and M components combined, $N = 231$) are the arithmetic mean (AM), median, geometric mean (GM), standard deviation (SD), maximum value (Max), and minimum value (Min).

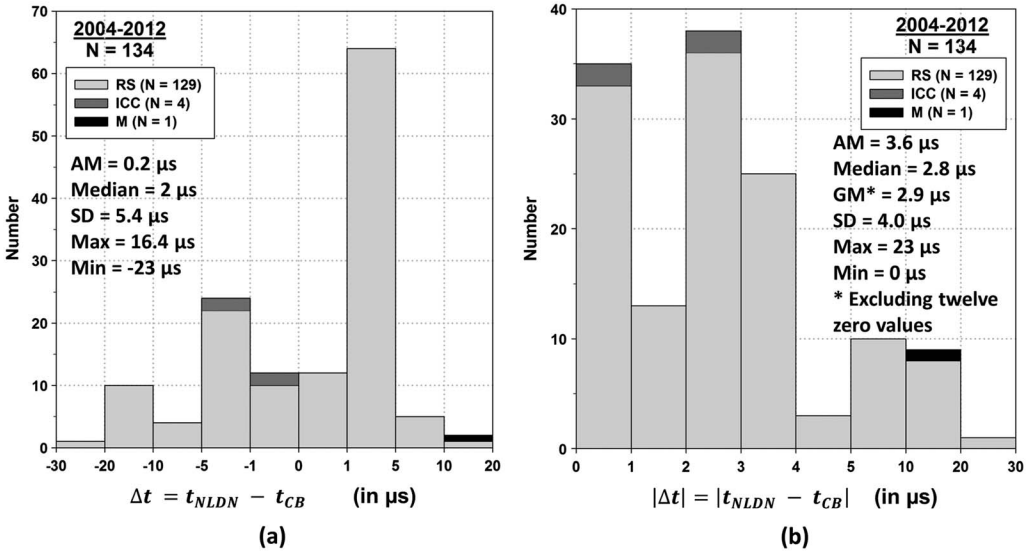

Figure 8. Histogram of (a) signed and (b) absolute event-time mismatch ($\Delta t = t_{NLDN} - t_{CB}$) for 134 events in 80 flashes triggered in 2004–2012. Different types of shading are used for return strokes (RS), ICC pulses (ICC), and M components (M). Statistics given (for return strokes, ICC pulses, and M components combined, $N = 134$) are the arithmetic mean (AM), median, geometric mean (GM), standard deviation (SD), maximum value (Max), and minimum value (Min).

Parameters of the nine detected superimposed pulses are given in Table 4. One of the detected ICC pulses (ICC1 of UF 09-42) occurred in one of the two flashes without return strokes (the other one was not detected by the NLDN). This is the only flash in our data set (with or without return strokes) that was detected via SIP. If we consider both flashes with return strokes (78) and without return strokes (2), the NLDN flash detection efficiency will be 93% (74/80) versus 94% (73/78) for only flashes with return strokes (see section 4.1).

4.3. Percentage of Misclassified Events

In 2004–2012, 9 (4%) out of 245 return strokes were misclassified by the NLDN as cloud (IC) discharges. Parameters of the nine misclassified strokes are summarized in Table 5. The median values of peak current,

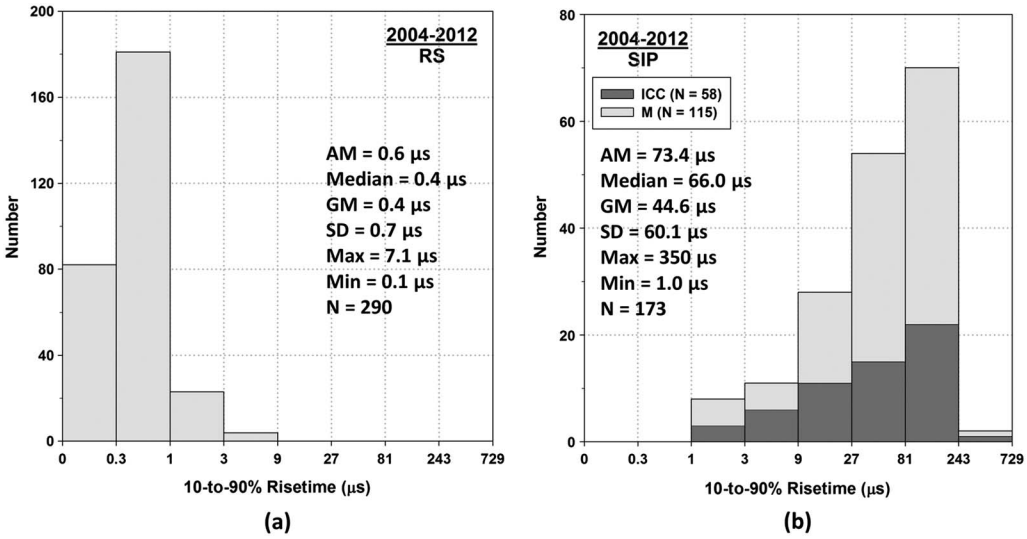

Figure 9. Histograms of 10 to 90% risetimes for (a) return strokes and (b) kiloampere-scale superimposed pulses, both detected and not detected by the NLDN. Statistics given are the arithmetic mean (AM), median, geometric mean (GM), standard deviation (SD), maximum value (Max), and minimum value (Min). *N* is the sample size.

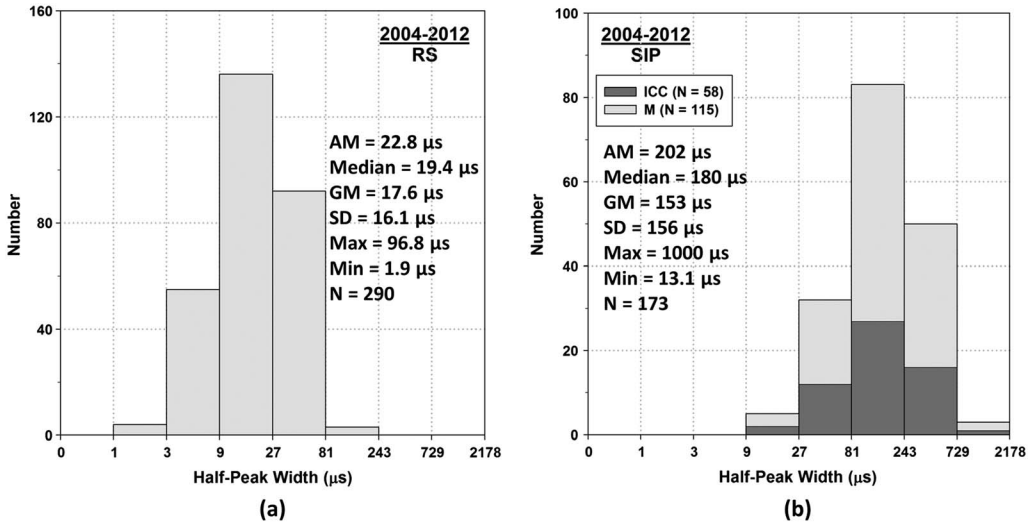

Figure 10. Histograms of half-peak widths for (a) return strokes and (b) kiloampere-scale superimposed pulses, both detected and not detected by the NLDN. Statistics given are the arithmetic mean (AM), median, geometric mean (GM), standard deviation (SD), maximum value (Max), and minimum value (Min). *N* is the sample size.

10 to 90% risetime, and half-peak width for four of these strokes are 10.3 kA, 0.55 μs, and 20 μs, respectively, all of which are similar to the corresponding values for "normal" return strokes in triggered lightning.

All nine superimposed pulses detected by the NLDN were correctly classified as cloud-to-ground (CG) events. Thus, the percentage of misclassified superimposed pulses is zero, although the NLDN makes no distinction between superimposed pulses and return strokes.

4.4. Location Accuracy

Figure 4 shows spatial distribution of locations for the 254 NLDN-detected events in 80 flashes triggered at Camp Blanding during 2004–2012. The origin of coordinates corresponds to the actual event location. The horizontal and vertical axes correspond to the east-west (east being positive) and north-south (north being positive) location error components, respectively.

For return strokes (RS) only, the arithmetic mean (AM) and median north-south location errors are 50 m and −109 m, respectively, while the AM and median east-west location errors are −247 m and −232 m, respectively. For all events (including RS, ICC, and M), the AM and median north-south location errors are 25 m and −109 m, respectively, while the AM and median east-west location errors are −234 m and −228 m, respectively.

Figure 5 shows the histogram of NLDN location errors (Δr) for the 254 events from 2004 to 2012. For return strokes only, the median location error is 334 m. For all events (including RS, ICC, and M), the median location error is 340 m. The largest location error is 8 km, and it corresponds to a return stroke. *Nag et al.* [2011] had reported a median location error of 308 m and a maximum of 4.2 km for 2004–2009. *Jerauld et al.* [2005] had reported a median location error of 600 m and a maximum of 11 km for 2001–2003. The median location error for 2004–2012 is slightly higher than that reported for 2004–2009 [*Nag et al.*, 2011] but lower than that reported for 2001–2003 [*Jerauld et al.*, 2005].

About 90% (228 out of 254) of events (including RS, ICC pulses, and M components) have location errors ≤1 km. Interestingly, 19 out of 26 events with location errors >1 km are from 2010–2012. It appears that the location accuracy during 2004–2009 was better than that during 2010–2012 (see section 5.7 for more discussion).

4.5. Peak Current Estimation Error

Figure 6 shows a scatter plot of the NLDN-estimated peak current versus peak current measured directly at Camp Blanding for 231 events in 80 flashes triggered in 2004–2012. The diagonal is the locus of the points for which the NLDN-reported peak current is equal to the Camp Blanding (directly measured) peak current.

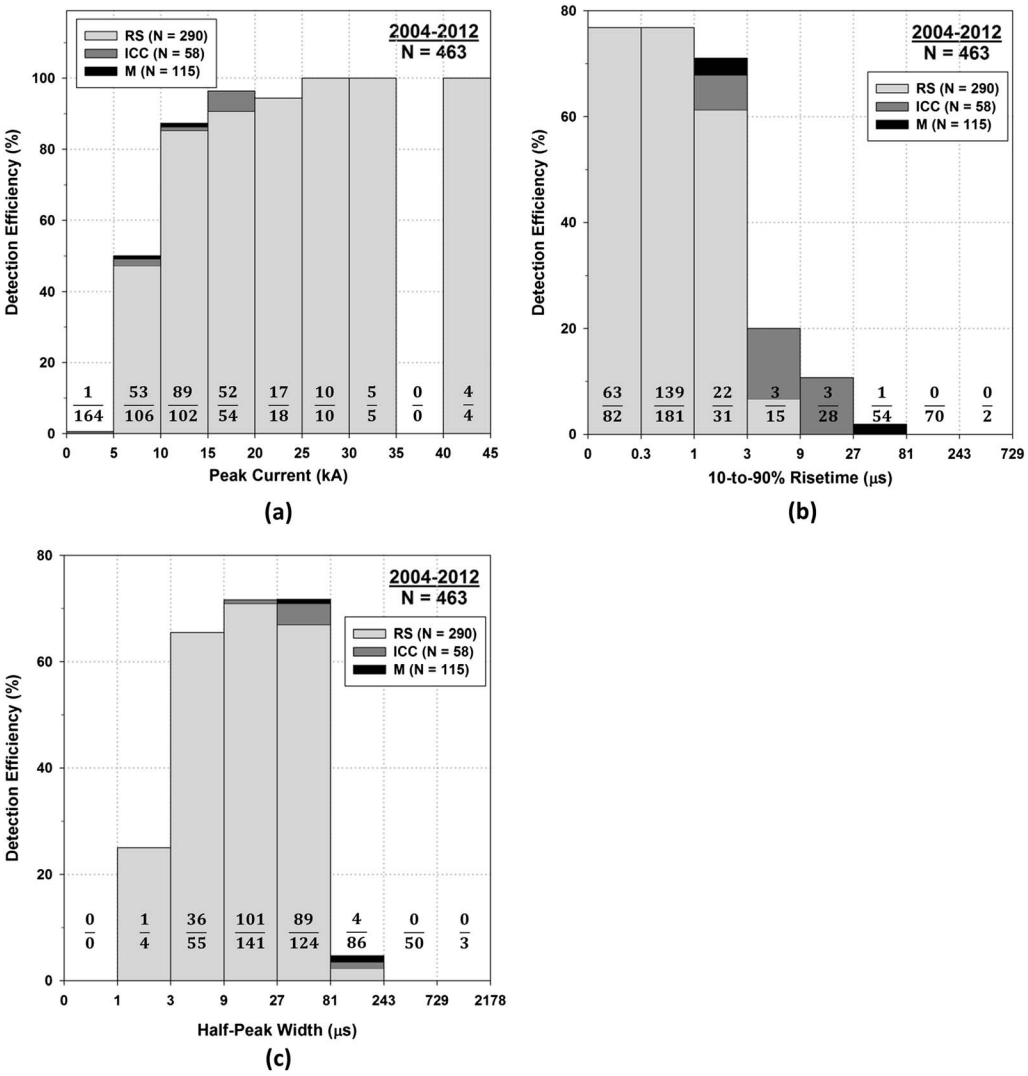

Figure 11. NLDN detection efficiency for both return strokes and kiloampere-scale superimposed pulses combined as a function of (a) peak current, (b) 10 to 90% risetime, and (c) half-peak width. For each histogram bin, the ratio given inside the column indicates the number of events detected by the NLDN (numerator) and the number of events recorded at Camp Blanding (denominator).

For 222 return strokes both reported by the NLDN and having directly measured currents, the GM of Camp Blanding peak current is 13.6 kA versus 12.5 kA for NLDN-reported peak currents. For all the 231 NLDN-reported events (including RS, ICC, and M) with directly measured currents, the GM of Camp Blanding peak current is 13.5 kA versus 12.3 kA for NLDN-reported peak currents. For all the 231 events, the AM value of the ratio I_{CB}/I_{NLDN} for 2004–2012 is 1.1. A greater than 1 ratio indicates that the NLDN tends to underestimate the peak current (by about 10%, on average, in 2004–2012). The AM of I_{CB}/I_{NLDN} ratio was 1.1 in 2004–2009 [*Nag et al.*, 2011] and 1.2 in 2001–2003 [*Jerauld et al.*, 2005].

Figure 7a shows a histogram for signed values of NLDN peak current estimation errors as a percentage of Camp Blanding peak current ($\Delta I\% = 100\Delta I/I_{CB}$, where $\Delta I = I_{NLDN} - I_{CB}$) for the 231 events (including RS, ICC, and M) from 2004–2012. For return strokes only, the AM and median values of $\Delta I\%$ are −5.6% and −5.0%, respectively. For all the events (including RS, ICC, and M), the AM and median values of $\Delta I\%$ are −5.9% and −5.4%, respectively. Since the distribution appears to be normal, the mean value and the standard deviation can be interpreted as systematic (−5%) and random (23%) error components. Figure 7b shows a histogram for the absolute values of NLDN peak current estimation errors ($|\Delta I|$) as a percentage of Camp Blanding

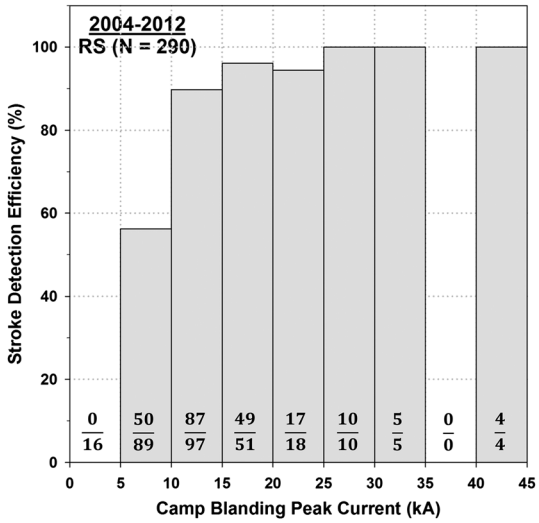

Figure 12. NLDN detection efficiency for 290 return strokes in 78 flashes triggered in 2004–2012 as a function of peak current directly measured at Camp Blanding. The ratio given inside each column indicates the number of strokes detected by the NLDN (numerator) and the number of strokes recorded at Camp Blanding (denominator).

peak current. For return strokes only, the AM and median values of $|\Delta I\%|$ are 17% and 14%, respectively. For all the events (including RS, ICC, and M), the AM and median values of $|\Delta I\%|$ are also 17% and 14%, respectively. The maximum value of $|\Delta I\%|$ is 127% and corresponds to a return stroke. The AM and median values of $|\Delta I\%|$ for return strokes in 2004–2009 were 17% and 13%, respectively [*Nag et al.*, 2011], whereas the AM and median values for return strokes in 2001–2003 were both 20% [*Jerauld et al.*, 2005].

4.6. Event-Time Mismatch

Figure 8a shows a histogram for the signed values of event-time mismatch (Δt) for 134 events (including RS, ICC, and M) in 80 flashes triggered at Camp Blanding during 2004–2012. For return strokes only, the AM and median values of Δt are 0.2 μs and 2 μs, respectively. For all events (including RS, ICC, and M), the AM and median values of Δt are also 0.2 μs and 2 μs, respectively. Figure 8b shows a histogram for the absolute values

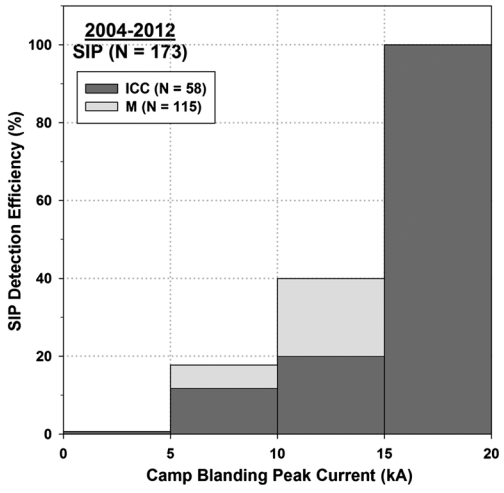

Peak Current Range (kA)	Detection Efficiency		
	ICC	M	SIP (ICC + M)
0 – 5*	2% (1/45)	0% (0/103)	1% (1/148)
5 –10	25% (2/8)	11% (1/9)	18% (3/17)
10 –15	50% (1/2)	33% (1/3)	40% (2/5)
15 –20	100% (3/3)	- (0/0)	100% (3/3)
0 –20	12% (7/58)	2% (2/115)	5% (9/173)

*Actually 1 – 5 kA.

Figure 13. NLDN detection efficiency for 173 SIPs in 80 flashes triggered in 2004–2012 as a function of peak current directly measured at Camp Blanding. For each peak current range (bin size of 5 kA), the ratio given in the parentheses in the table indicates the number of pulses detected by the NLDN (numerator) and the number of pulses recorded at Camp Blanding (denominator) for that peak current range. Note that the majority of events in the 0–5 kA (actually 1–5 kA) range are M components and that all three events in the 15–20 kA range are ICC pulses.

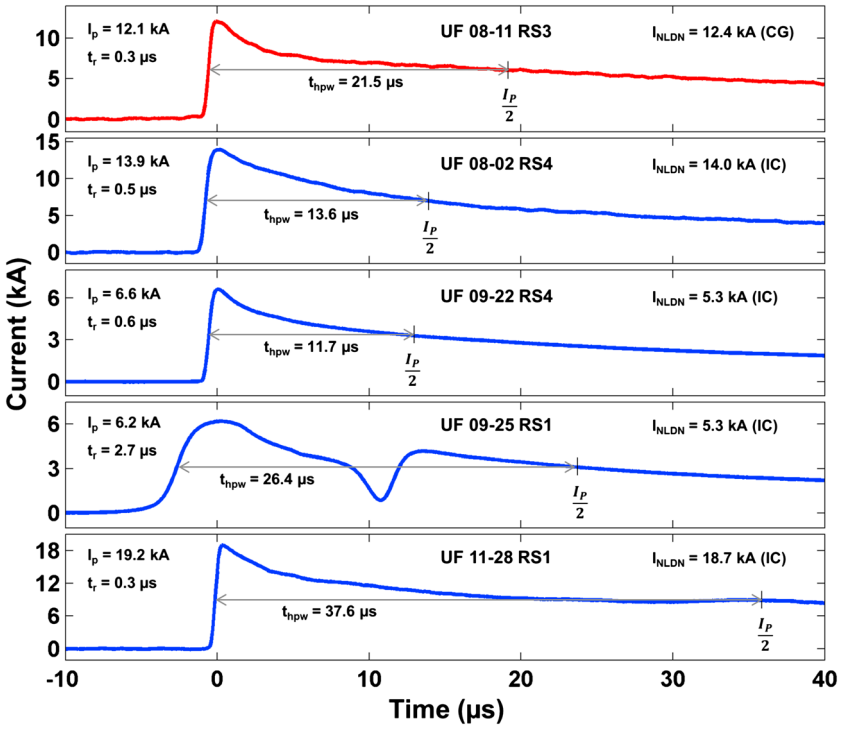

Figure 14. Comparison of negative return-stroke current waveforms correctly and incorrectly classified by the NLDN. (first panel) The channel-base current for a typical return stroke which was correctly reported by the NLDN as cloud-to-ground (CG) discharge. (second to fifth panels) The channel-base currents of four return strokes which were incorrectly reported by the NLDN as cloud (IC) discharges. Here, I_P is the peak value of current pulse, t_r is the 10 to 90% risetime, t_{hpw} is the half-peak width, and I_{NLDN} is the peak current estimated by the NLDN.

of event-time mismatch ($|\Delta t|$). For return strokes only, the AM and median values of $|\Delta t|$ are 3.6 μs and 2.8 μs, respectively. For all events (including RS, ICC, and M), the AM and median values of $|\Delta t|$ are also 3.6 μs and 2.8 μs, respectively. The maximum value of $|\Delta t|$ is 23 μs and corresponds to a return stroke. For 114 (85%) out of the 134 events (including RS, ICC pulses, and M components), the event-time mismatch is ≤5 μs.

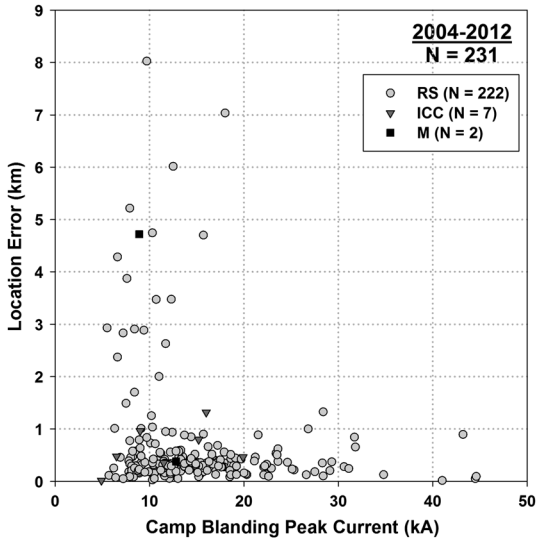

Figure 15. NLDN location error versus peak current directly measured at Camp Blanding for both return strokes and kiloampere-scale superimposed pulses.

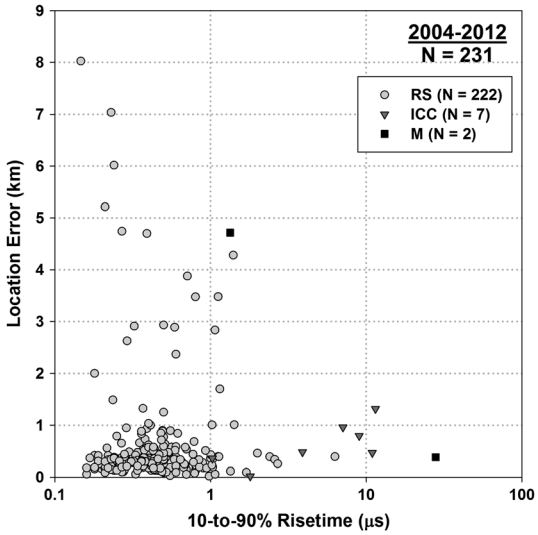

Figure 16. NLDN location error versus 10 to 90% risetime for both return strokes and kiloampere-scale superimposed pulses.

5. Discussion

5.1. Detection Efficiency

In this section, we examine how (or if) the event (return stroke or superimposed pulse) detection efficiency is influenced by the current waveform parameters: peak value, 10 to 90% risetime, and half-peak width. We first consider distributions of these three parameters for all the events recorded at Camp Blanding in 2004–2012, both detected and not detected by the NLDN.

Histograms of peak currents for 290 return strokes and 173 superimposed pulses are shown in Figures 3a and 3b, respectively. For return-stroke peak currents, the AM is 13.1 kA, the GM is 11.5 kA, median is 11.7 kA, maximum is 44.6 kA, and minimum is 2.0 kA. For peak currents of superimposed pulses, the AM is 3.0 kA, the GM is 2.3 kA, median is 1.9 kA, maximum is 19.9 kA, and minimum (selected cutoff) is 1.0 kA. Figure 9 shows histograms of 10 to 90% risetimes (t_r) for 290 return strokes and 173 superimposed pulses recorded during 2004–2012 and Figure 10 shows histograms of half-peak widths (t_{hpw}) for the same events. Clearly, superimposed pulses typically have longer risetimes and half-peak widths than return strokes do, while peak currents are larger for return strokes than for superimposed pulses.

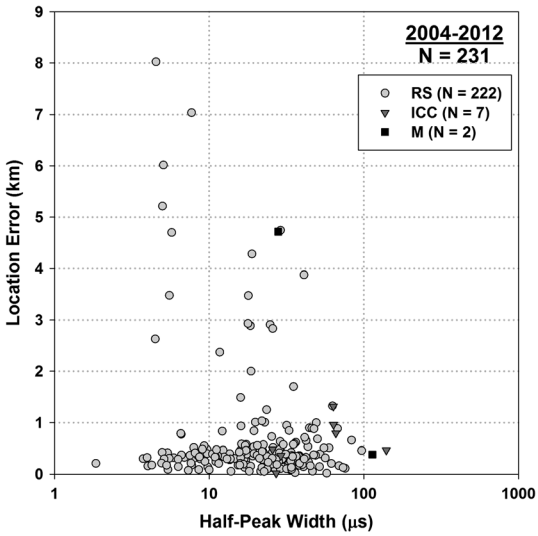

Figure 17. NLDN location error versus half-peak width for both return strokes and kiloampere-scale superimposed pulses.

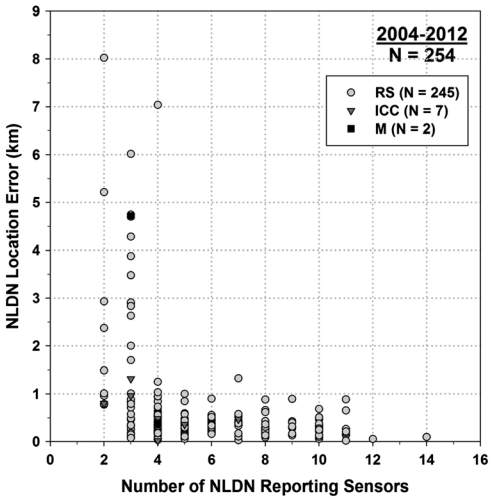

Number of Sensors	Location Error (km)				N
	AM	Median	Min	Max	
2	2.44	1.25	0.77	8.02	10
3	1.69	0.86	0.07	6.02	36
4	0.48	0.32	0.02	7.04	62
5	0.34	0.32	0.06	1.00	51
6	0.35	0.31	0.16	0.90	24
7	0.42	0.39	0.03	1.33	16
8	0.32	0.27	0.09	0.88	20
9	0.36	0.31	0.13	0.89	8
10	0.29	0.27	0.06	0.68	17
11	0.31	0.20	0.02	0.89	8
12	-	-	0.06	0.06	1
13	-	-	-	-	0
14	-	-	0.10	0.10	1
2 – 14	0.65	0.34	0.02	8.02	254

Figure 18. NLDN location error versus the number of reporting NLDN sensors for both return strokes and kiloampere-scale superimposed pulses. Note that the maximum number of sensors used for location was 10. Statistics for each number of reporting sensors and for all data combined are given in the table.

We examined correlation between the parameters, although the corresponding scatter plots are not shown here. It appears that there is no correlation between either risetime or half-peak width and the peak current, which is true for both return strokes (in confirmation of previous findings of *Fisher et al.* [1993]) and superimposed pulses (in confirmation of the previous findings for M components of *Thottappillil et al.* [1995]). On the other hand, there appears to be a tendency for increasing half-peak width of the superimposed pulse with increasing its risetime, which is not seen for return strokes.

Figure 11 shows the NLDN detection efficiency as a function of (a) peak current, (b) risetime, and (c) half-peak width for both return strokes and kiloampere-scale superimposed pulses combined. It is evident that the chances of a pulse being detected by the NLDN are generally higher for events having peak currents above 10 kA, half-peak widths in the range of 3 to 81 μs, and risetimes less than 3 μs. Figure 12 additionally shows the NLDN detection efficiency as a function of peak current for return strokes only, just to facilitate direct comparison with previous studies [*Jerauld et al.*, 2005; *Nag et al.*, 2011]. The return-stroke detection efficiency is 100% for peak currents above 25 kA and decreases to 56% for strokes in the 5 to 10 kA range. None of the 16 strokes with peak currents ≤5 kA was detected by the NLDN which is in agreement with results of *Jerauld et al.* [2005] and *Nag et al.* [2011].

The overall flash and return-stroke detection efficiencies were 94% and 75%, respectively. For comparison, the flash detection efficiency in Southern Arizona was estimated by *Biagi et al.* [2007] to be 93% ($N = 1097$) and in Texas/Oklahoma it was 92% ($N = 367$). The corresponding stroke detection efficiencies were 76% ($N = 3620$) and 86% ($N = 882$).

The NLDN detected a total of nine kiloampere-scale superimposed pulses, including seven ICC pulses and two M components (see Table 4). All the NLDN-detected superimposed pulses were correctly reported as cloud-to-ground events, although they were not distinguished from return strokes. The NLDN apparently detected these superimposed pulses because they had relatively large peak currents, short risetimes, and short half-peak widths. Figure 13 shows the NLDN detection efficiency for superimposed pulses as a function of peak current directly measured at Camp Blanding. The pulse detection efficiency is 100% for peak currents above 15 kA and decreases with decreasing peak current (more abruptly than for return strokes; see Figure 12). Interestingly, one ICC pulse with a peak current of 4.9 kA was detected by the NLDN, while none of the 16 return-stroke pulses with peaks ≤5 kA was detected.

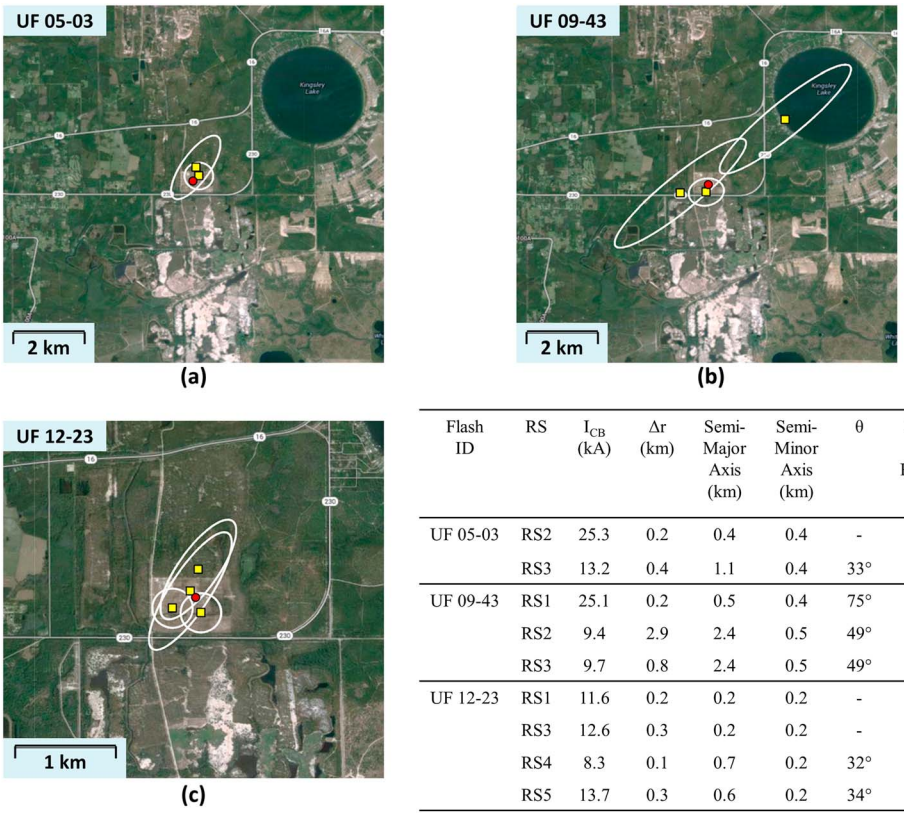

Flash ID	RS	I_{CB} (kA)	Δr (km)	Semi-Major Axis (km)	Semi-Minor Axis (km)	θ	Number of Reporting Sensors
UF 05-03	RS2	25.3	0.2	0.4	0.4	-	10
	RS3	13.2	0.4	1.1	0.4	33°	4
UF 09-43	RS1	25.1	0.2	0.5	0.4	75°	6
	RS2	9.4	2.9	2.4	0.5	49°	3
	RS3	9.7	0.8	2.4	0.5	49°	3
UF 12-23	RS1	11.6	0.2	0.2	0.2	-	9
	RS3	12.6	0.3	0.2	0.2	-	5
	RS4	8.3	0.1	0.7	0.2	32°	3
	RS5	13.7	0.3	0.6	0.2	34°	4

Figure 19. Examples of 50% location error ellipses (some are actually circles) for all strokes detected by the NLDN in three different flashes (a) UF 05-03, (b) UF 09-43, and (c) UF 12-23. Flash UF 05-03 had four return strokes, and the NLDN detected two of them, RS2 and RS3. Flash UF 09-43 had five return strokes, and the NLDN detected three of them, RS1, RS2, and RS3. Flash UF 12-23 had five return strokes, and the NLDN detected four of them, RS1, RS3, RS4, and RS5. The red circle corresponds to the actual stroke location, and the centers of ellipses (shown by yellow squares) correspond to stroke locations reported by the NLDN. I_{CB} is the peak value of current directly measured at Camp Blanding, Δr is the location error, and θ is the ellipse angle (with respect to north). Note that the spatial scale in Figure 19c is different from that in Figures 19a and 19b.

It is possible that some if not all of the NLDN-detected SIPs are associated with the mixed mode of charge transfer to ground [*Zhou et al.*, 2011], where the leader/return-stroke sequence occurs in one branch, while the initial continuous current flows to ground in another branch. We examined the available optical (high-speed video, standard high-definition (HD) video, and still camera) records of the flashes in which superimposed pulses were detected by the NLDN, to see if there was any evidence of upward branching below the cloud base. The results are presented in the last column of Table 4. In two out of the nine cases, there was optical evidence of a descending leader coming in contact with the grounded channel within a few hundred meters of the rocket launcher (see section 5.6 for more discussion).

5.2. Misclassified Events

The NLDN reported 9 (4%) out of 245 return strokes as cloud discharges. All the available information on these misclassified events is summarized in Table 5. Overall, the misclassified events appear unremarkable. Current waveforms are available for only four misclassified return strokes, and those are shown in Figure 14. For these four return strokes, peak currents ranged from 6.2 to 19.2 kA (median = 10.3 kA), current 10 to 90% risetimes ranged from 0.3 to 2.7 μs (median = 0.6 μs), and current half-peak widths ranged from 11.7 to 37.6 μs (median = 20 μs). The corresponding ranges for all the 218 return strokes correctly identified by the NLDN as CGs are 5.5 to 44.6 kA (median = 13.1 kA) for peak currents, 0.1 to 6.3 μs (median = 0.4 μs) for risetimes, and 1.9 to 96.7 μs (median = 22.7 μs) for half-peak widths. Only in one case (UF 09-25 RS1) does the current waveform not have the characteristics of a typical return-stroke current waveform. After the current peak, the current abruptly drops and then rises again (see Figure 14, fourth panel). Further analysis is required to explain the reasons why the NLDN misidentified these return strokes as cloud discharges. We plan to

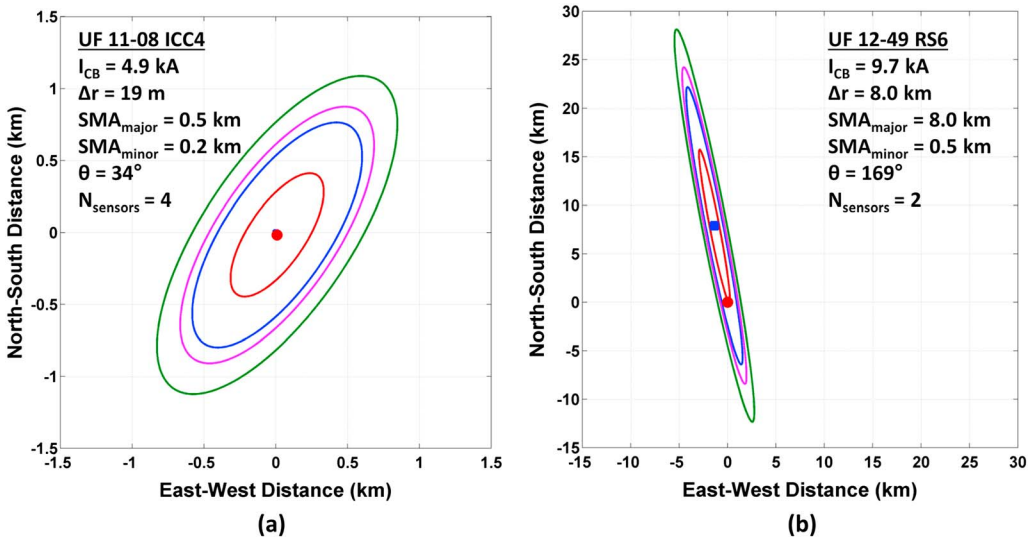

Figure 20. Illustration of 50% (red), 90% (blue), 95% (magenta), and 99% (green) location error ellipses estimated by the NLDN. (a) Event UF 11-08 ICC4 which has the smallest location error of 19 m and (b) event UF 12-49 RS6 which has the largest location error of 8 km. The origin of coordinates (shown by red circle) corresponds to the actual stroke location, and the centers of ellipses (shown by blue square, which coincides with the red circle in (a)) correspond to stroke locations estimated by the NLDN. I_{CB} is peak value of current directly measured at Camp Blanding, Δr is the location error, SMA_{major} is the semimajor axis length of 50% error ellipse, SMA_{minor} is the semiminor axis length of 50% error ellipse, θ is the ellipse angle (with respect to north), and $N_{sensors}$ is the number of NLDN reporting sensors.

examine the corresponding electric field waveforms measured at the Lightning Observatory in Gainesville [*Rakov et al.*, 2014], Florida, located at a distance of 45 km from Camp Blanding.

Biagi et al. [2007], using video cameras, investigated the classification of lightning events as IC or CG discharges by the NLDN in Southern Arizona, Oklahoma, and Texas during 2003 and 2004. A similar study was done by *Fleenor et al.* [2009] (who additionally used Los Alamos Sferic Array (LASA) electric field waveform measurements) in the Colorado-Kansas-Nebraska region in 2005. *Warner et al.* [2012], using video cameras to study upward flashes from towers in South Dakota, found that out of 151 superimposed pulses and subsequent return strokes reported by the NLDN, 70% were correctly classified as −CGs and 30% were misclassified as ICs. The latter figure (30%) is considerably higher than 4% (for return strokes only) resulted from our study.

5.3. Location Accuracy

The median location error (340 m) found in our study for all events combined is somewhat larger than 206 m reported by *Warner et al.* [2012] for 151 events in upward flashes initiated from towers in South Dakota. The corresponding largest errors are 8 km and about 2 km.

Figure 15 shows the NLDN location error plotted versus peak current directly measured at Camp Blanding for both return strokes and kiloampere-scale superimposed pulses recorded during 2004–2012. The overwhelming majority, 228 (90%) out of 254 events (including return strokes, ICC pulses, and M components), are located with errors ≤1 km. Almost all (36 out of 37) events with peak currents >20 kA are associated with location errors ≤1 km, with the only one exception being a return stroke with peak current of 28.4 kA and location error of 1.3 km. A total of 26 (10%) events have location errors >1 km, most of them (22 out of 26) with peak currents ≤15 kA. The largest location error of 8 km corresponds to a return stroke having peak current of 9.7 kA. Figures 16 and 17 show the NLDN location error versus 10 to 90% risetime and half-peak width, respectively. It appears that events with large location errors tend to be associated with relatively short risetimes and relatively small half-peak widths. Interestingly, the majority (19 out of 26) of events with location errors >1 km occurred in flashes triggered during 2010–2012 (see section 5.7 for more discussion).

Table 6. Percentage of Events Whose Actual Location is Enclosed by Location Error Ellipses Reported by the NLDN for Different Confidence Levels and Different Observation Periods[a]

Ellipse Confidence Level	Percentage of Events Inside the Ellipse										
	2004 ($N = 9$)	2005 ($N = 8$)	2007 ($N = 1$)	2008 ($N = 31$)	2009 ($N = 59$)	2010 ($N = 42$)	2011 ($N = 26$)	2012 ($N = 78$)	2004–2009 ($N = 108$)	2010–2012 ($N = 146$)	2004–2012 ($N = 254$)
50%	100	100	100	77	83	71	27	55	84	55	67
90%	100	100	100	100	98	90	46	94	99	84	91
95%	100	100	100	100	100	90	46	97	100	86	92
99%	100	100	100	100	100	95	69	99	100	92	96

[a]There was no lightning triggered in 2006 at Camp Blanding. The minimum reportable length of semimajor axis (SMA) of the 50% location error ellipse was 400 m in 2004–2010, and it was 200 m in 2011–2012.

Figure 18 shows the NLDN location error versus the number of NLDN reporting sensors. The number of reporting sensors ranges from 2 to 14, although the maximum number of sensors used for location is 10. The mean number of reporting sensors for both return strokes and kiloampere-scale superimposed pulses is 6. The location error tends to decrease as the number of reporting sensors increases, which is expected. For all events, except for one, location errors do not exceed 1 km when the number of reporting sensors is 5 or more. The exception is the return stroke (already noted above) with peak current of 28.4 kA and location error of 1.3 km, which was detected by seven sensors.

In the following, we will examine location error ellipses reported by the NLDN. According to *Vaisala Inc* [2004], the NLDN 50% error ellipse is calculated for each stroke location and defined as a confidence region for which there is a 50% probability that the actual stroke location lies within the area circumscribed by the ellipse, with the center of the ellipse being the most probable (reported) stroke location. The semimajor axis of the 50% ellipse is usually viewed as the median (50%) location error. Corresponding error ellipses for any probability level can be derived by multiplying the semimajor and semiminor axes of the 50% ellipse by an appropriate scaling factor. The scaling factors are 1.82, 2.08, and 2.58 for probability levels of 90%, 95%, and 99%, respectively. The ellipse angle is the orientation of the semimajor axis relative to north. A similar description of NLDN error ellipses was given by *Nag et al.* [2011]. We largely repeat their description here in order to make this paper self-contained.

In order to illustrate shapes and sizes of NLDN error ellipses, in Figure 19 we show 50% location error ellipses for all NLDN located strokes in three rocket-triggered flashes. Further, relative sizes of 50%, 90%, 95%, and 99% error ellipses are illustrated in Figure 20 for event UF 11-08 ICC4 (Figure 20a) which has the smallest location error of 19 m and event UF 12-49 RS6 (Figure 20b) which has the largest location error of 8 km. Event UF 11-08 ICC4 corresponds to an ICC pulse with peak current of 4.9 kA, semimajor axis length of 0.5 km, and number of reporting sensors of 4. The actual stroke location is enclosed by 50% error ellipse reported by the NLDN. Event UF 12-49 RS6 corresponds to a return stroke with peak current of 9.7 kA, semimajor axis length of 8 km, and number of NLDN reporting sensors of 2. The actual stroke location is not enclosed by the 50% error ellipse but is enclosed by the 90% one.

Table 6 gives the percentage of events whose actual location is enclosed by error ellipses reported by the NLDN for different confidence levels. For the 35 events with semimajor axis lengths >1 km, 74% (26 of 35) and 91% (32 of 35) have the actual stroke location enclosed by the 50% and 90% error ellipse, respectively. For all data combined, 67% of events are inside the 50% ellipse and 91% inside the 90% ellipse. For 95% and 99% ellipses, the percentages of events inside the ellipses are 92% and 96%, respectively. Events from 2011 were more often outside the lower confidence level error ellipses. It appears that the NLDN-reported location ellipses are generally consistent with observations.

For 254 events (including return strokes, ICC pulses, and M components), the median of semimajor axis length of the 50% location error ellipse,

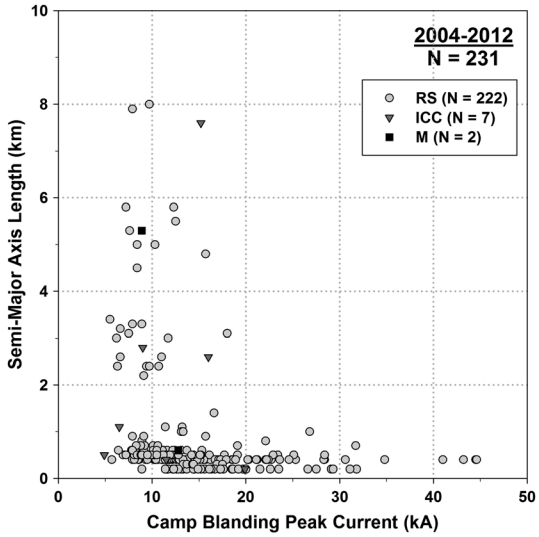

Figure 21. Semimajor axis length of NLDN 50% location error ellipse versus peak current directly measured at Camp Blanding for both return strokes and kiloampere-scale superimposed pulses.

which is often viewed as the median location error, is 0.4 km. This value is comparable with the median location error of 0.34 km estimated using the ground truth data. For return strokes only, these two measures of location errors are 0.4 km and 0.33 km, respectively. Note that prior to 28 December 2010, the minimum reportable length of the semimajor axis of the 50% error ellipse had been 0.4 km and that it was reduced to 0.2 km after that date.

Figure 21 shows the NLDN 50% semimajor axis lengths versus peak current directly measured at Camp Blanding. Semimajor axis lengths of ≤1 km were reported for 86% of the events (219 of 254). A total of 35 (14%) events have semimajor axis length >1 km, for 33 of which directly measured currents are available. For 28 of the 33 events with semimajor axis length >1 km, peak currents were ≤15 kA. The largest semimajor axis length was 8 km for a return stroke having a peak current of 9.7 kA (the same event that is associated with the largest location error).

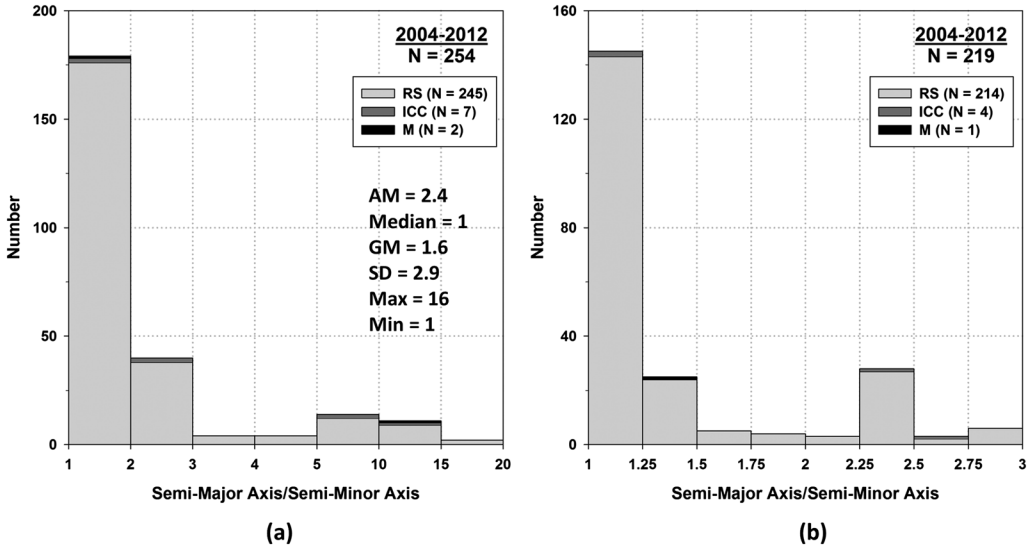

Figure 22. Histograms of ratio of semimajor to semiminor axis lengths of NLDN 50% location error ellipses for both return strokes and kiloampere-scale superimposed pulses for (a) all data ($N = 254$) and (b) events with the ratio less than 3 ($N = 219$).

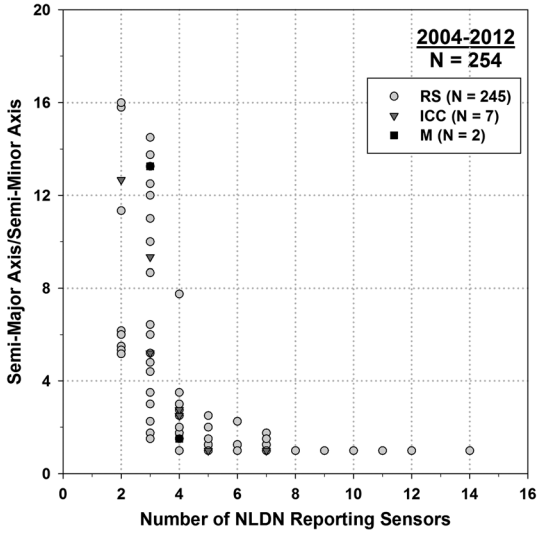

Figure 23. Ratio of semimajor to semiminor axis lengths of NLDN error ellipses versus number of reporting NLDN sensors for return strokes and kiloampere-scale superimposed pulses.

Figure 22 shows a histogram of the ratio of semimajor to semiminor axis lengths for NLDN location error ellipses. More than one half (145 out of 254 or 57%) of events have nearly circular error ellipses (ratio ≤1.25). Figure 23 shows the ratio of semimajor to semiminor axis lengths of NLDN error ellipses plotted versus number of reporting NLDN sensors. As expected, events with larger ratios were reported by a few NLDN sensors.

Figure 24 shows a histogram of location error ellipse angles for 118 events for which this parameter could be determined. For 136 out of 254 events, error ellipses were essentially circular and, hence, not suitable for this analysis. It appears that angles in two out of six sectors occur considerably more often. The reasons for this are presently not clear. It is worth noting that the ellipse angle at a particular location depends upon the position of the NLDN sensors relative to that location (in this case Camp Blanding) and, hence, is specific to that location.

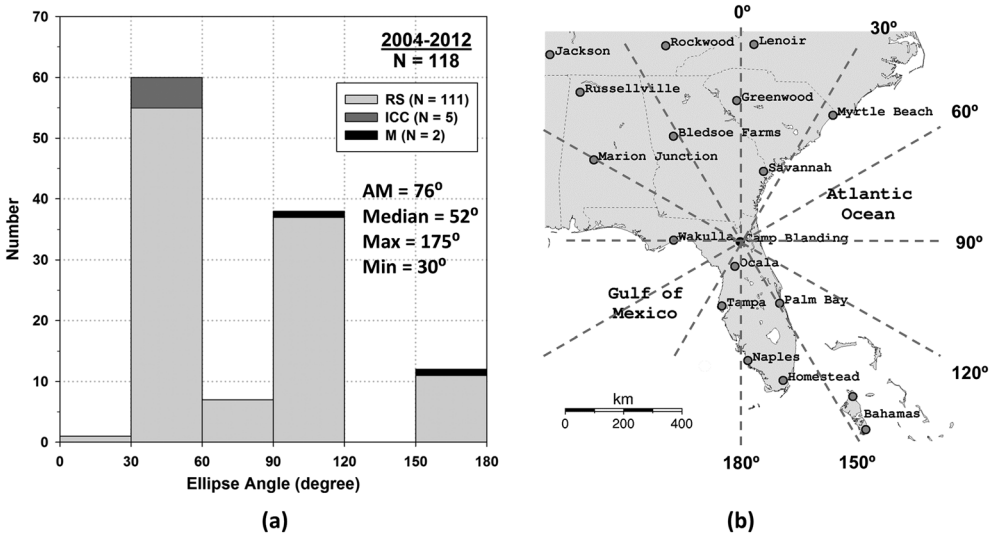

Figure 24. (a) Histogram of NLDN location error ellipse angles for both return strokes and kiloampere-scale superimposed pulses and (b) reference map. Note that 136 out of 254 events have essentially circular error ellipses and, hence, are not included in the histogram.

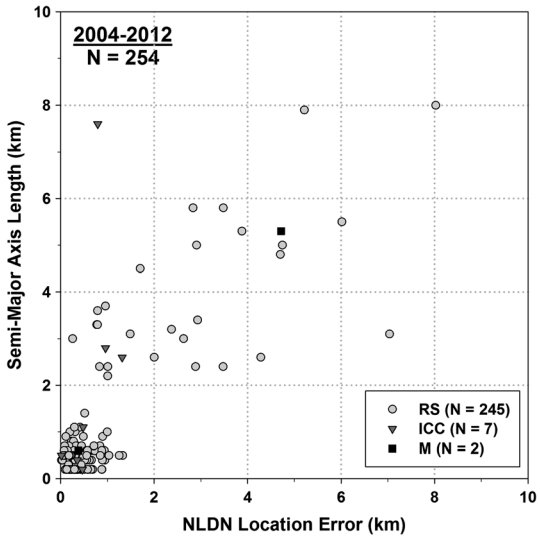

Figure 25. NLDN 50% location error ellipse semimajor axis length versus NLDN location error for return strokes and kiloampere-scale superimposed pulses.

Figure 25 shows the NLDN 50% semimajor axis length versus NLDN location error. Strokes having location errors ≤1 km are typically associated with semimajor axis lengths of ≤1 km. It is worth noting that all the 35 events with the semimajor axis lengths >1 km have elongated (as opposed to nearly circular) error ellipses.

Generally, data from the NLDN sensors are used to produce an optimum lightning location based on the chi-squared minimization technique [*Hiscox et al.*, 1984; *Cummins et al.*, 1993]. The chi-squared value corresponding to the optimum (reported) location is a measure of consistency of data from all participating sensors. According to *Vaisala Inc* [2004], chi-squared values ≤3 are considered as good values and chi-squared values in the range of 3–10 are considered as acceptable. Chi-squared values of >10 are attributed to poorly calibrated sensors, high noise level, or miscorrelations in time, and these are considered by Vaisala as "outliers".

Figure 26 shows a histogram of chi-squared values for 254 events (including RS, ICC, and M) recorded in 2004–2012. The overwhelming majority (244 out of 254 or 96%) of events have very good chi-squared values ≤3. Out of the 10 events with chi-squared values >3, 9 events have an acceptable chi-squared value

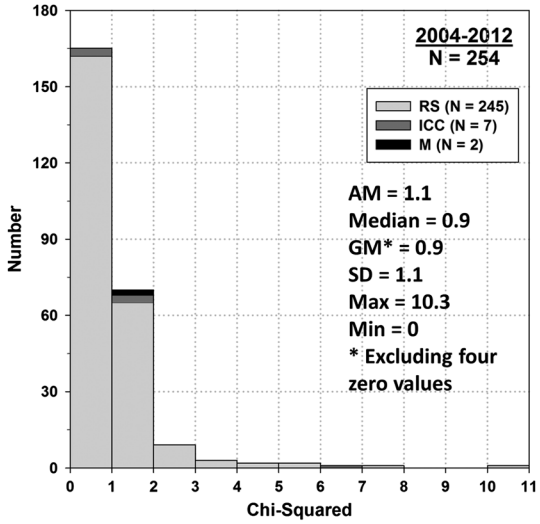

Figure 26. Histogram of chi-squared value for both return strokes and kiloampere-scale superimposed pulses.

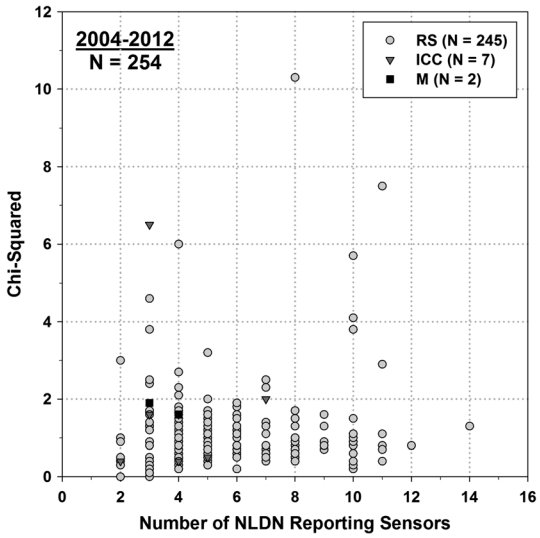

Figure 27. Chi-squared value versus number of reporting NLDN sensors for return strokes and kiloampere-scale superimposed pulses.

in the range of 3–10 and 1 event has a chi-squared value of 10.3. It is interesting to note that only one event (out of 108) had a chi-squared value >3 (3.2) in 2004–2009, whereas in 2010–2012 nine events (out of 146) had chi-squared value >3 (see section 5.7 for more discussion). The median chi-squared value is 0.9 both for all events combined ($N = 254$) and for return strokes only ($N = 245$).

Figure 27 shows the chi-squared value plotted versus number of reporting NLDN sensors for return strokes and kiloampere-scale superimposed pulses. No clear trend is seen in this figure; that is, relatively large values of chi-squared can be associated with either small or large number of reporting sensors. The event with largest chi-squared value was reported by eight NLDN sensors.

Figure 28 shows the NLDN location error versus chi-squared value for both return strokes and kiloampere-scale superimposed pulses. We do not observe any clear trend in this figure. The event with the largest location error (8 km) corresponds to a very good chi-squared value of 0.5.

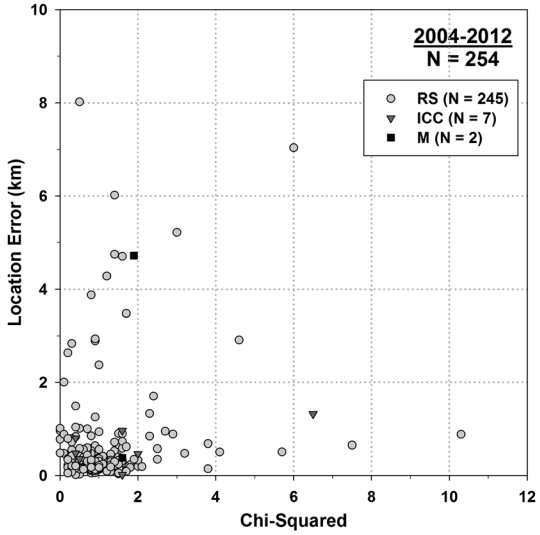

Figure 28. NLDN location error versus chi-squared value for return strokes and kiloampere-scale superimposed pulses.

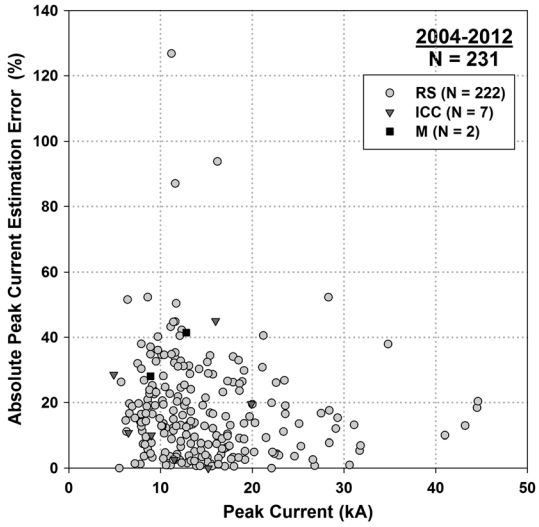

Figure 29. Absolute NLDN peak current estimation error versus peak current directly measured at Camp Blanding for both return strokes and kiloampere-scale superimposed pulses.

5.4. Peak Current Estimates

Figure 29 shows the absolute NLDN peak current estimation error versus the peak current directly measured at Camp Blanding for both return strokes and kiloampere-scale superimposed pulses recorded in 2004–2012. In general, the upper bound of current estimation error tends to decrease with increasing peak current. We also examined the absolute NLDN peak current estimation error versus 10 to 90% risetime and versus half-peak width and found no clear trends.

Figure 30 shows the absolute NLDN peak current estimation error versus the number of reporting NLDN sensors. Interestingly, the largest (>80%) errors are associated with events reported by a relatively large number of sensors (8 to 10).

Figure 31 shows the absolute NLDN peak current estimation error versus chi-squared value for return strokes and kiloampere-scale superimposed pulses. The largest absolute peak current estimation errors are associated with small chi-squared values.

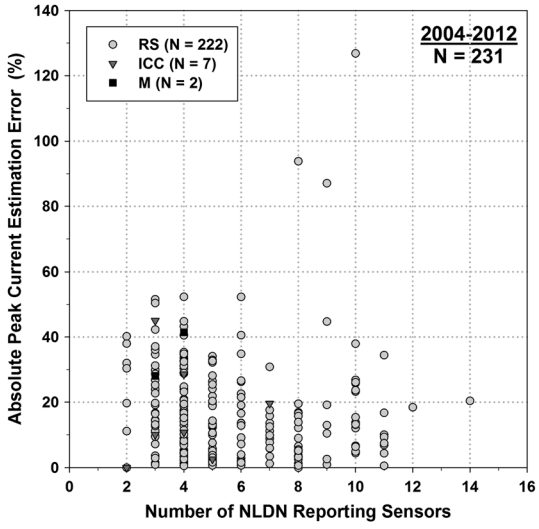

Figure 30. Absolute NLDN peak current estimation error versus the number of reporting sensors for both return strokes and kiloampere-scale superimposed pulses.

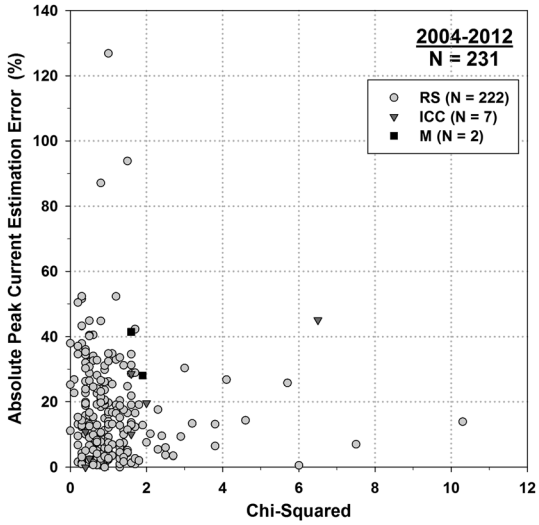

Figure 31. Absolute NLDN peak current estimation error versus chi-squared value for return strokes and kiloampere-scale superimposed pulses.

5.5. Event-Time Mismatch

Figure 32 shows the absolute event-time mismatches versus the number of reporting NLDN sensors. The largest mismatches ($>10\,\mu s$) are associated with relatively small numbers (2 to 4) of reporting NLDN sensors, with one exception for which the number of reporting sensors is 9.

Figure 33 shows the NLDN location error versus the absolute event-time mismatch. It is expected that the location error should be correlated with the event-time mismatch. It appears from Figure 33 that relatively large event-time mismatches are generally associated with relatively large location errors. Indeed, 13 out of the 20 events with event-time mismatches $>5\,\mu s$ have location errors >1 km, and the event with the largest event-time mismatch of $23\,\mu s$ has the largest location error of 8 km. The correlation coefficient between location error and absolute event-time mismatch is 0.81 for all the 134 events and 0.56 for 16 events with mismatches $>7\,\mu s$. In Figure 33, there are 16 events with event-time mismatches $>7\,\mu s$. Thirteen of them are accompanied by large (>1 km) location errors, but three are not. All the 13 events with large ($>7\,\mu s$) event-time mismatches and large (>1 km) location errors occurred in flashes triggered in 2011 and 2012 (mostly in

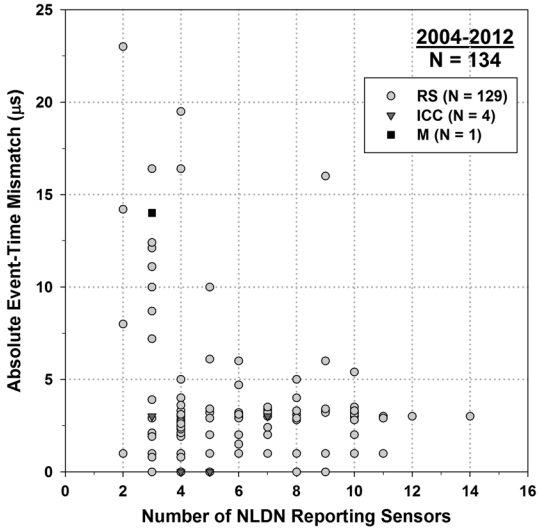

Figure 32. Absolute event-time mismatch versus the number of reporting NLDN sensors for both return strokes and kiloampere-scale superimposed pulses.

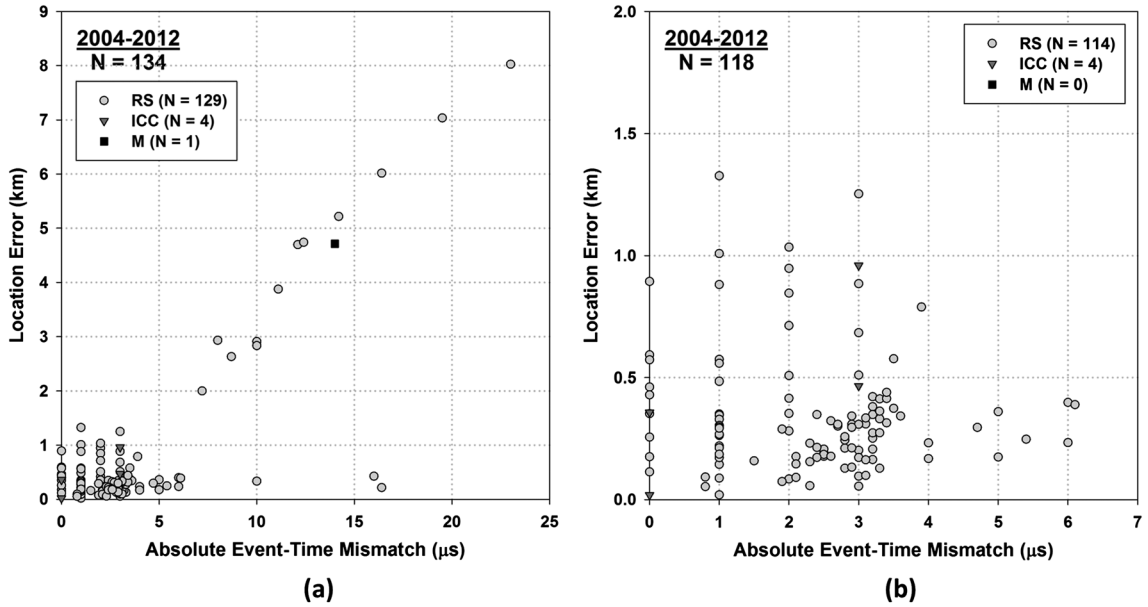

Figure 33. NLDN location error versus absolute event-time mismatch for both return strokes and kiloampere-scale superimposed pulses for (a) all 134 events and (b) 114 events with absolute event-time mismatches ≤7 μs and location errors ≤2 km (see Figure S1 and Table S1 in supporting information for more details).

2012; see Figure S1 and Table S1 in supporting information). Note that in 2010–2012, the NLDN was undergoing an upgrade, including changes influencing the arrival time measurements (see section 2). Characteristics of the 13 events with large (>7 μs) time mismatches and large (>1 km) location errors, for which the correlation coefficient is 0.98, are summarized in Table 7. The median values of Camp Blanding peak current and 10 to 90% risetime for these 13 events are 9.7 kA and 0.29 μs, respectively, versus 11.7 kA and 0.41 μs for 290 return strokes recorded at Camp Blanding in 2004–2012.

5.6. Superimposed Pulses and Upward Branching

We examined the available optical (high-speed video, standard HD video, and still camera) records of the flashes in which superimposed pulses were detected by the NLDN, to see if there was any evidence of

Table 7. Summary of 13 Events With Large (>7 μs in Absolute Value) Event-Time Mismatches and Large (>1 km) Location Errors

Flash ID	RS/SIP ID	Δt (μs)	I_{CB} (kA)	I_{NLDN} (kA)	ΔI (%)	SMA[a] (km)	Δr (km)	t_r (μs)	t_{hpw} (μs)	Chi-squared	Number of Reporting Sensors
UF 11-08	RS4	8.0	5.5	5.5	0	3.4	2.9	0.5	17.8	0.9	2
UF 11-18	RS1	−10	8.4	9.6	14	5.0	2.9	0.32	24.8	4.6	3
UF 11-20	RS1	−10	7.2	7.1	−1.3	5.8	2.8	1.07	25.8	0.3	3
UF 11-35	M1 (RS2)	14	8.9	6.4	−28	5.3	4.7	1.34	28.0	1.9	3
UF 12-35	RS9	−20	18.0	17.9	−0.6	3.1	7.0	0.23	7.69	6.0	4
UF 12-43	RS1	−14	7.9	5.5	−30	7.9	5.2	0.21	4.99	3.0	2
UF 12-49	RS3	−16	12.5	8.6	−31	5.5	6.0	0.24	5.06	1.4	3
UF 12-49	RS4	−12	15.7	11.2	−29	4.8	4.7	0.39	5.72	1.6	3
UF 12-49	RS6	−23	9.7	5.8	−40	8.0	8.0	0.15	4.53	0.5	2
UF 12-49	RS7	8.7	11.7	5.8	−50	3.0	2.6	0.29	4.48	0.2	3
UF 12-54	RS2	−11	7.6	9.1	20	5.3	3.9	0.71	41.0	0.8	3
UF 12-54	RS3	−12	10.3	10.6	2.9	5.0	4.7	0.27	28.9	1.4	3
UF 12-55	RS4	7.2	11.0	8.5	−23	2.6	2.0	0.18	18.7	0.1	3
	AM	−6.9	10.3	8.6	−15	5.0	4.4	0.50	16.7	1.7	3
	Median	−11	9.7	8.5	−23	5.0	4.7	0.29	17.8	1.4	3
	N	13	13	13	13	13	13	13	13	13	13

[a]SMA is the semimajor axis length of the NLDN 50% location error ellipse.

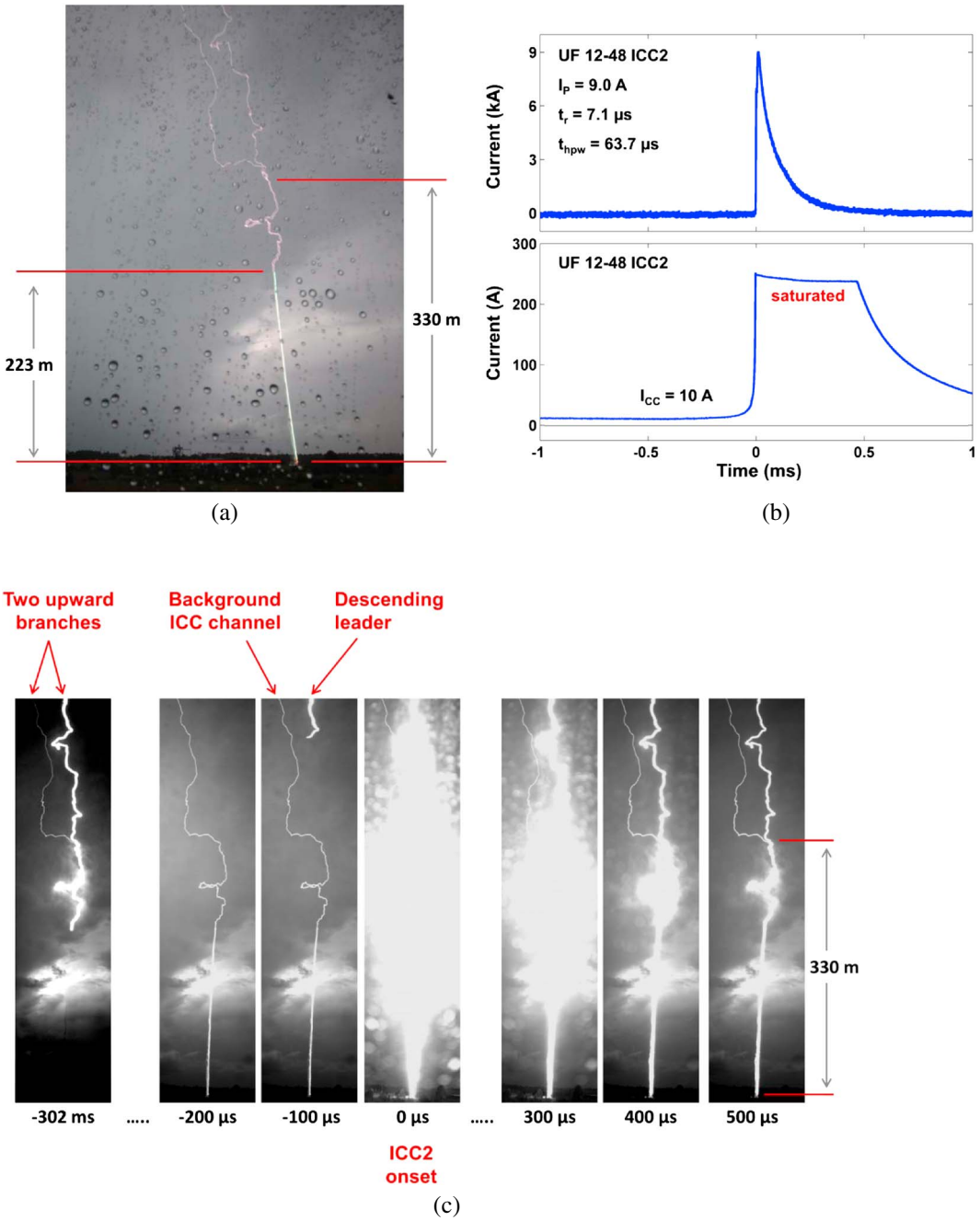

Figure 34. (a) Still camera (5 s exposure) record showing upward branching of lightning channel for flash UF 12-48. The straight portion of the bottom of the lightning channel indicates the length of the triggering wire at the time of its explosion. (b) Channel-base current of ICC2 in flash UF 12-48 (top, current measured in the 0–60 kA range; bottom, current measured in the 0–250 A range). (c) Image-enhanced frames of high-speed (100 µs per frame) video record showing a reilluminated branch (descending leader) coming in contact with the grounded channel and giving rise to the ICC pulse. The branching point is 330 m above the top of the rocket launcher. The reilluminated branch was first visible when the initial stage of UF 12-48 started at $t = -302$ ms and then decayed (became faintly luminous, practically not visible at $t = -200$ µs). Note that the luminosity of the background ICC channel appears to be not influenced by the occurrence of ICC2.

upward branching below the cloud base. Relatively low-level (a few hundred meters above the channel termination point) upward branches are known to be associated with superimposed pulses that exhibit characteristics similar to those of return-stroke pulses [*Flache et al.*, 2008; *Zhou et al.*, 2011]. In two out of the nine cases, there was optical evidence of such branching.

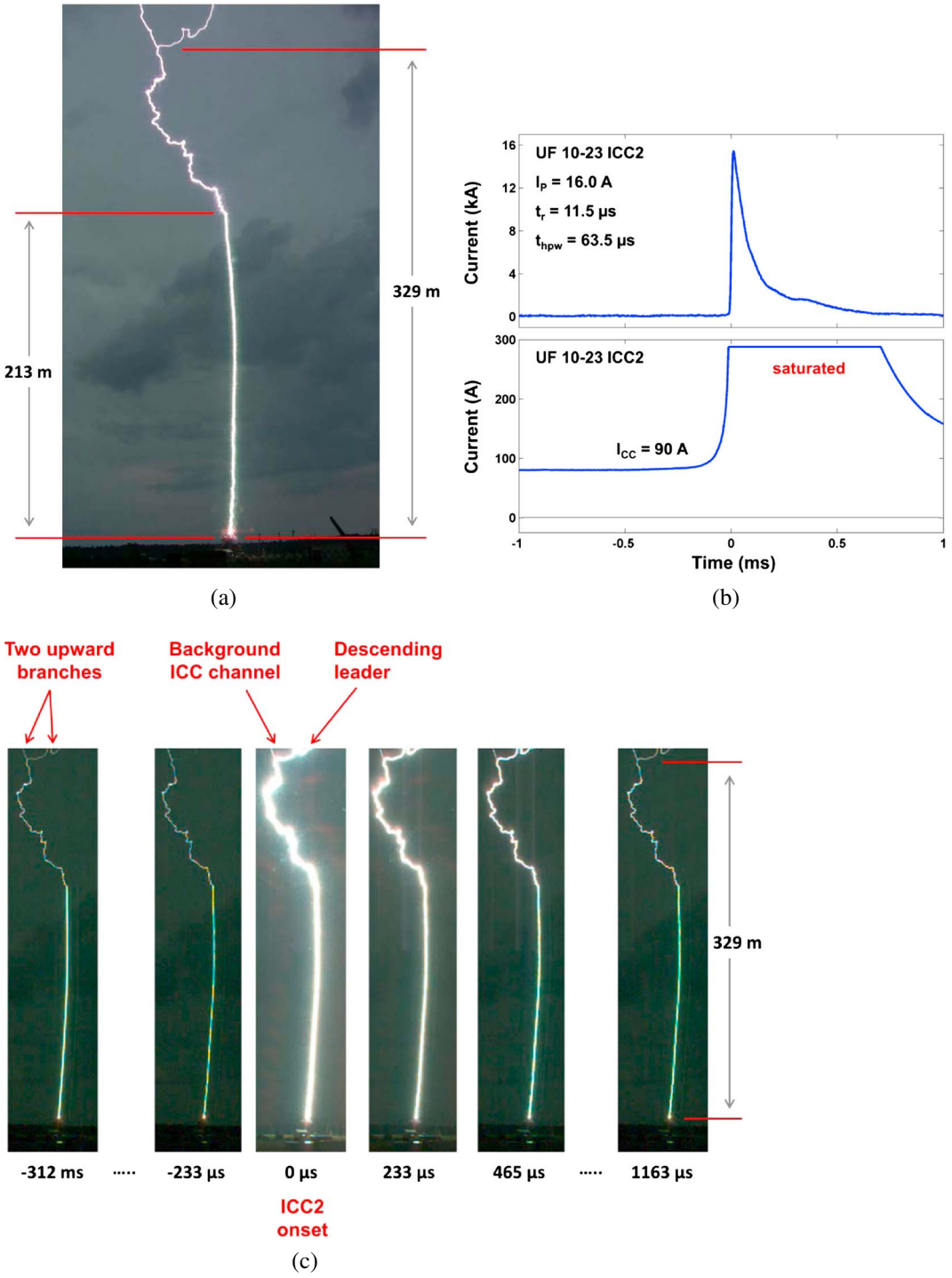

Figure 35. (a) Frame of HD Video (30 fps) record showing upward branching of lightning channel for flash UF 10-23. The nearly straight portion of the bottom of the lightning channel indicates the length of the triggering wire at the time of its explosion. (b) Channel-base current of ICC2 in flash UF 10-23 (top, current measured in the 0–70 kA range; bottom, current measured in the 0–300 A range). (c) Image-enhanced frames of high-speed (233 μs per frame) video record showing a reilluminated branch (by inference descending leader) coming in contact with the grounded channel and giving rise to the ICC pulse. The branching point is 329 m above the top of the rocket launcher. The reilluminated branch was first visible in our high-speed video record at $t = -312$ ms and then decayed (became faintly luminous, practically not visible at $t = -233$ μs). Note that from the current records, the initial stage of UF 10-23 started at $t = -340$ ms, while the first frame of the high-speed video record corresponds to $t = -312$ ms.

Table 8. Comparison of NLDN Performance Characteristics for Return Strokes and Kiloampere-Scale (≥ 1 kA) Superimposed Pulses Recorded in 2004–2009 and 2010–2012

Observation Period			2004–2009	2010–2012	2004–2012
Detection efficiency	Flashes with RS		89%	98%	94%
	RS		77%	74%	75%
	SIP		4%	6%	5%
	RS + SIP		51%	51%	51%
Percentage of misclassified events	RS		6%	2%	4%
	SIP		0%	0%	0%
	RS + SIP		6%	2%	4%
Location error	RS	Median	310 m	343 m	334 m
		Max	4.3 km	8.0 km	8.0 km
	SIP	Median	481 m	713 m	481 m
		Max	0.8 km	4.7 km	4.7 km
	RS + SIP	Median	323 m	347 m	340 m
		Max	4.3 km	8.0 km	8.0 km
Absolute current estimation error	RS	Median	13%	14%	14%
		Max	127%	87%	127%
	SIP	Median	11%	24%	20%
		Max	41%	45%	45%
	RS + SIP	Median	13%	14%	14%
		Max	127%	87%	127%
Event-time mismatch	RS	Median	1 μs	2.9 μs	2.8 μs
		Max	16 μs	23 μs	23 μs
	SIP	Median	-	3 μs	3 μs
		Max	-	14 μs	14 μs
	RS + SIP	Median	1 μs	2.9 μs	2.8 μs
		Max	16 μs	23 μs	23 μs
50% location error ellipse semimajor axis length	RS	Median	0.4 km	0.4 km	0.4 km
		Max	4.5 km	8.0 km	8.0 km
	SIP	Median	1.1 km	1.6 km	1.1 km
		Max	7.6 km	5.3 km	7.6 km
	RS + SIP	Median	0.4 km	0.4 km	0.4 km
		Max	7.6 km	8.0 km	8.0 km
Ratio of semimajor to semiminor axis lengths	RS	Median	1.0	1.0	1.0
		Max	6.4	16.0	16.0
	SIP	Median	2.8	3.9	2.8
		Max	12.7	13.3	13.3
	RS + SIP	Median	1.0	1.0	1.0
		Max	12.7	16.0	16.0
Median value of location error ellipse angle	RS		88°	85°	87°
	SIP		53°	72°	53°
	RS + SIP		88°	85°	87°
Chi-squared	RS	Median	0.9	0.8	0.9
		Max	3.2	10.3	10.3
	SIP	Median	0.4	1.8	1.6
		Max	1.6	6.5	6.5
	RS + SIP	Median	0.9	0.8	0.9
		Max	3.2	10.3	10.3
Average number of reporting sensors	RS		6	6	6
	SIP		3	4	4
	RS + SIP		6	5[a]	6

[a]This value differs from that (6) given in Table 3, last row, because the sample used here additionally includes events without directly measured currents.

Figure 34a shows a still camera image for flash UF 12-48, in which upward branching is seen at 330 m above the launcher (107 m above the top of the wire channel section). Current records for ICC2 of UF 12-48 are shown on two vertical scales in Figure 34b. Figure 34c shows image-enhanced frames of high-speed (10,000 fps or 100 μs per frame) video record prior to, during, and after the occurrence of the ICC2. The steady current (flowing in the left branch and common channel section below the branching point) prior to the onset of ICC2 had a magnitude of 10 A (see Figure 34b, bottom). A descending leader developed in the

Table 9. Comparison of Performance Characteristics of the NLDN for Return Strokes Evaluated for 2001–2003 [*Jerauld et al.*, 2005], 2004–2009 [*Nag et al.*, 2011], and 2004–2012 (Present Study)

Reference	*Jerauld et al.* [2005]	*Nag et al.* [2011]	Present Study
Time period	2001–2003	2004–2009	2004–2012
Number of flashes with return strokes	37	37	78
Number of strokes	159	139	326
Flash detection efficiency	84%	92%	94%
Stroke detection efficiency	60%	76%	75%
Misclassified events	-	-	4%
Median location error	600 m	308 m	334 m
Median absolute current estimation error	20%	13%	14%
Median absolute event-time mismatch	-	-	2.8 μs
Median chi-squared	-	-	0.9

previously luminous but decayed right branch and made contact with the existing grounded channel. The resultant ICC pulse had a peak of 9 kA (see Figure 34b, top).

Figure 35a shows a frame of regular HD video (30 fps) record of flash UF 10-23 with upward branching 329 m above the launcher (116 m above the top of wire channel section). Current records for ICC2 of UF10-23 are shown in Figure 35b. Figure 35c shows image-enhanced frames of high-speed (4300 fps or 233 μs per frame) video record prior to, during, and after the occurrence of ICC2. The steady current (flowing in the left branch and common channel section below the branching point) prior to the onset of ICC2 was 90 A (see Figure 34b, bottom), and the ICC pulse had a peak of 16 kA (see Figure 35b, top). ICC2 occurs when the previously luminous but decayed right branch becomes reilluminated, probably via a descending leader coming in contact with the existing grounded channel, as in the case of ICC2 of flash UF12-48 shown in Figure 34.

In both UF 12-48 and UF 10-23, the ICC pulses were associated with reillumination of previously luminous branches and, hence, likely resulted from recoil leaders in decayed branches, as opposed to independently initiated leaders coming in contact with the grounded channel [*Yoshida et al.*, 2012].

For the remaining seven superimposed pulses which were detected by the NLDN, no evidence of upward branching was found below the photographed altitudes of 290 to 400 m above the launcher (see the last column of Table 4). There is, however, a possibility of upward branching occurring at altitudes greater than 290 to 400 m above the launcher (outside the vertical field of view of the cameras). Typical cloud base heights during Florida thunderstorms are about 1 ± 0.5 km, so that undetected upward branching could have occurred below the cloud base, although such branching is rare for summer lightning triggered at nearly sea level in Florida and China [*Qie et al.*, 2011]. *Hill et al.* [2012], from their analysis of VHF lightning channel images, reported that in eight out of nine Camp Blanding flashes the first branching occurred at altitudes ranging from 580 m to about 5.2 km (in most cases above 1.1 km).

Unfortunately, the available optical data are very limited and do not allow a detailed analysis of the relation between SIP parameters and upward branching that could potentially shed some light on differences between return strokes, ICC pulses, and M components. Using Peissenberg Tower observations in Germany, *Flache et al.* [2008] analyzed simultaneous current and high-speed video records for 33 ICC pulses and 9 M components in 2 upward positive and 6 upward negative flashes. They found that both ICC pulses and M components with longer 10 to 90% risetimes (>8 μs) tended to occur in already luminous channels (showing no branching within the field of view of their camera, up to 350 m above the tower top) and hence were interpreted as indicative of the M component mode of charge transfer to ground [*Rakov et al.*, 2001]. On the other hand, pulses with shorter 10 to 90% risetimes (<8 μs) tended to involve a newly illuminated, low-altitude (less than 350 m above the tower top) branch and were attributed to the leader/return-stroke mode in that branch. In the latter case, because of the presence of background steady current supplied by the other branch, *Zhou et al.* [2011] referred to the entirety of processes in both branches and in the common channel section below the branching point as the mixed mode of charge transfer to ground. For the two ICC pulses examined in this paper, 10 to 90% risetimes were 7.1 and 11.5 μs.

Table 10. Comparison of the Detection Efficiencies and Median Location Errors for Individual Years from 2004 to 2012[a]

	2004	2005	2007	2008	2009	2010	2011	2012	2004–2009	2010–2012	2004–2012
Number of flashes	3	8	1	7	17	12	11	19	36	42	78
Number of strokes	13	13	2	37	72	50	38	101	137	189	326
Flash detection efficiency (%)	100	63	100	100	94	100	100	95	89	98	94
Stroke detection efficiency (%)	69	62	50	81	79	80	61	76	77	74	75
Median location error (m)	135	242	55	362	326	381	652	258	310	343	334

[a]There was no lightning triggered at Camp Blanding in 2006.

5.7. Comparison of NLDN Performance Characteristics for Different Time Periods

Nag et al. [2013a] reported on the NLDN upgrade in 2010–2012 and completed in 2013. In that upgrade, the NLDN LS7001 and IMPACT sensors were replaced with newer generation LS7002 sensors designed to improve the location accuracy. Details of the upgrades to both the sensor and associated algorithm are given by *Cummins et al.* [2012] and *Honma et al.* [2013]. In this section, we compare the NLDN performance characteristics for the periods before (2004–2009) and during (2010–2012) the upgrade.

Table 8 shows the NLDN performance characteristics for the two periods, 2004–2009 and 2010–2012. There are minor differences in some values given in Table 8 for 2004–2009 and those previously reported by *Nag et al.* [2011] for the same period due to data reprocessing (see section 3). It is evident from Table 8 that the median location error for 2010–2012 is slightly higher than that for 2004–2009.

Table 9 gives the NLDN performance characteristics for the three periods, 2001–2003 [*Jerauld et al.*, 2005], 2004–2009 [*Nag et al.*, 2011], and 2004–2012 (present study).

Table 10 gives the detection efficiencies and median location errors for individual years from 2004 to 2012. One can see that the NLDN performance characteristics listed in this table for 2010–2012 are about the same as their counterparts for 2004–2009. The median location error was the largest (652 m) in 2011, which, at least in part, is related to the problem with propagation corrections discussed in section 2.

6. Summary

The performance characteristics of the U.S. National Lightning Detection Network (NLDN) evaluated using, as the ground truth, rocket-triggered lightning data acquired in 2004–2012 at Camp Blanding, Florida, are presented. The overall data set consists of 78 flashes containing both the initial stage and leader/return-stroke sequences and 2 flashes composed of the initial stage only. These 80 flashes contain a total of 326 return strokes (directly measured channel-base currents are available for 290 of them) and 173 kiloampere-scale (≥1 kA) superimposed pulses (58 initial continuous current pulses and 115 M components). All the events transported negative charge to ground. The NLDN detected 245 return strokes and 9 superimposed pulses. The resultant flash detection efficiency is 94%, return-stroke detection efficiency is 75%, and the detection efficiency for superimposed pulses is 5% for peak currents ≥1 kA and 32% for peak currents ≥5 kA. For return strokes, the median location error is 334 m and the median value of absolute peak current estimation error is 14%. The corresponding values for superimposed pulses are 481 m and 20%. The percentage of misclassified events is 4%, all of them being return strokes. The median value of absolute event-time mismatch for return strokes is 2.8 μs.

Table 9 compares the NLDN performance characteristics for return strokes for three time periods, 2001–2003 [*Jerauld et al.*, 2005], 2004–2009 [*Nag et al.*, 2011], and 2004–2012 (present study). These results, based on using triggered-lightning data, are applicable only to negative subsequent return strokes in natural downward lightning (or flashes without first strokes in the case of flash detection efficiency, such as tower-initiated upward flashes).

The median value of chi-squared for return strokes and superimposed pulses are 0.9 and 1.6, respectively, with the corresponding average numbers of reporting sensors being 6 and 4, respectively. It appears that the NLDN-reported location error ellipses are generally consistent with observations. For two out of the nine superimposed pulses detected by the NLDN, we found optical evidence of a reilluminated branch (recoil leader) coming in contact with the existing grounded channel within a few hundred meters above the rocket launcher.

Acknowledgments
This research was supported in part by NSF grant ATM-0852869 and DARPA Grant HR0011-10-1-0061. The authors would like to thank K. L. Cummins who provided useful comments.

References

Berger, K. (1967), Novel observations on lightning discharges: Results of research on Mount San Salvatore, *J. Franklin Inst.*, *283*(6), 478–525, doi:10.1016/0016-0032(67)90598-4.

Biagi, C. J., K. L. Cummins, K. E. Kehoe, and E. P. Krider (2007), National Lightning Detection Network (NLDN) performance in southern Arizona, Texas, and Oklahoma in 2003–2004, *J. Geophys. Res.*, *112*, D05208, doi:10.1029/2006JD007341.

Cummins, K. L., and M. J. Murphy (2009), An overview of lightning locating systems: History, techniques, and data uses, with an in-depth look at the U.S. NLDN, *IEEE Trans. EMC*, *51*(3), 499–518, doi:10.1109/TEMC.2009.2023450.

Cummins, K. L., R. O. Burnett, W. L. Hiscox, and A. E. Pifer (1993), Line reliability and fault analysis using the National Lightning Detection Network, Preprint, *Proc. Conf. on Precise Measur. in Power Syst.*, II–4.1–15, Arlington, Va.

Cummins, K. L., M. J. Murphy, E. A. Bardo, W. L. Hiscox, R. B. Pyle, and A. E. Pifer (1998), A combined TOA/MDF technology upgrade of the U.S. National Lightning Detection Network, *J. Geophys. Res.*, *103*(D8), 9035–9044, doi:10.1029/98JD00153.

Cummins, K. L., M. J. Murphy, J. A. Cramer, W. Scheftic, N. Demetriades, and A. Nag (2010), Location accuracy improvements using propagation corrections: A case study of the U.S. National Lightning Detection Network, *Proc. 21st Int. Light. Detect. Conf. (ILDC)*, Orlando, Fla.

Cummins, K. L., N. Honma, A. E. Pifer, T. Rogers, and M. Tatsumi (2012), Improved detection of winter lightning in the Tohoku region of Japan using Vaisala's LS700x technology, *IEEJ Trans. Power Energy*, *132*(6), 529–535, doi:10.1541/ieejpes.132.529.

Diendorfer, G., H. Pichler, and M. Mair (2009), Some parameters of negative upward-initiated lightning to the Gaisberg Tower (2000–2007), *IEEE Trans. EMC*, *51*(3), 443–452, doi:10.1109/TEMC.2009.2021616.

Fisher, R. J., G. H. Schnetzer, R. Thottappillil, V. A. Rakov, M. A. Uman, and J. D. Goldberg (1993), Parameters of triggered-lightning flashes in Florida and Alabama, *J. Geophys. Res.*, *98*(D12), 22,887–22,902, doi:10.1029/93JD02293.

Flache, D., V. A. Rakov, F. Heidler, W. Zischank, and R. Thottappillil (2008), Initial-stage pulses in upward lightning: Leader/return stroke versus M-component mode of charge transfer to ground, *Geophys. Res. Lett.*, *35*, L13812, doi:10.1029/2008GL034148.

Fleenor, S. A., C. J. Biagi, K. L. Cummins, E. P. Krider, and X. Shao (2009), Characteristics of cloud-to-ground lightning in warm-season thunderstorms in the Central Great Plains, *Atmos. Res.*, *91*(2–4), 333–352, doi:10.1016/j.atmosres.2008.08.011.

Hill, J. D., J. Pilkey, M. A. Uman, D. M. Jordan, W. Rison, and P. Krehbiel (2012), Geometrical and electrical characteristics of the initial stage in Florida triggered lightning, *Geophys. Res. Lett.*, *39*, L09807, doi:10.1029/2012GL051932.

Hiscox, W. L., E. P. Krider, A. E. Pifer, and M. A. Uman (1984), A systematic method for identifying and correcting 'site errors' in a network of magnetic direction finders, Preprint, *Proc. Int. Aerosp. Ground Conf. on Light. and Static Electr.*, 7-1–5, Orlando, Fla.

Honma, N., K. L. Cummins, M. J. Murphy, A. E. Pifer, and T. Rogers (2013), Improved lightning locations in the Tohoku region of Japan using propagation and waveform onset corrections, *IEEJ Trans. Power Energy*, *133*(2), 195–202, doi:10.1541/ieejpes.133.195.

Jerauld, J., V. A. Rakov, M. A. Uman, K. J. Rambo, D. M. Jordan, K. L. Cummins, and J. A. Cramer (2005), An evaluation of the performance characteristics of the U.S. National Lightning Detection Network in Florida using rocket-triggered lightning, *J. Geophys. Res.*, *110*, D19106, doi:10.1029/2005JD005924.

McCann, G. D. (1944), The measurement of lightning currents in direct strokes, *Trans. AIEE*, *63*(12), 1157–1164, doi:10.1109/T-AIEE.1944.5058859.

Nag, A., et al. (2011), Evaluation of U.S. National Lightning Detection Network performance characteristics using rocket-triggered lightning data acquired in 2004–2009, *J. Geophys. Res.*, *116*, D02123, doi:10.1029/2010JD014929.

Nag, A., M. J. Murphy, A. E. Pifer, and J. A. Cramer (2013a), Performance characteristic improvements of the U.S. National Lightning Detection Network, *6th Conf. on the Meteorolog. Appl. of Light. Data*, abstract 4.5, Austin, Tex.

Nag, A., M. J. Murphy, K. L. Cummins, A. E. Pifer, and J. A. Cramer (2013b), Upgrade of the U.S. National Lightning Detection Network in 2013, *Proc. 2013 Int. Symp. on Light. Prot. (XII SIPDA)*, 80–84, Belo Horizonte, Braz.

Qie, X., R. Jiang, C. Wang, J. Yang, J. Wang, and D. Liu (2011), Simultaneously measured current, luminosity, and electric field pulses in a rocket-triggered lightning flash, *J. Geophys. Res.*, *116*, D10102, doi:10.1029/2010JD015331.

Rakov, V. A., and M. A. Uman (2003), *Lightning: Physics and Effects*, Cambridge Univ. Press, New York.

Rakov, V. A., D. E. Crawford, K. J. Rambo, G. H. Schnetzer, and M. A. Uman (2001), M-component mode of charge transfer to ground in lightning discharges, *J. Geophys. Res.*, *106*(D19), 22,817–22,831, doi:10.1029/2000JD000243.

Rakov, V. A., S. Mallick, A. Nag, and V. B. Somu (2014), Lightning Observatory in Gainesville (LOG), Florida: A review of recent results, *Electr. Power Syst. Res.*, doi:10.1016/j.epsr.2014.02.037.

Thottappillil, R., J. D. Goldberg, V. A. Rakov, and M. A. Uman (1995), Properties of M components from currents measured at triggered lightning channel base, *J. Geophys. Res.*, *100*(D12), 25,711–25,720, doi:10.1029/95JD02734.

Vaisala Inc. (2004), Introduction to lightning detection, Tech. Note M210573EN-A, Tucson, Ariz.

Warner, T. A., K. L. Cummins, and R. E. Orville (2012), Upward lightning observations from towers in Rapid City, South Dakota and comparison with National Lightning Detection Network data, 2004–2010, *J. Geophys. Res.*, *117*, D19109, doi:10.1029/2012JD018346.

Yoshida, S., et al. (2012), The initial stage processes of rocket-and-wire triggered lightning as observed by VHF interferometry, *J. Geophys. Res.*, *117*, D09119, doi:10.1029/2012JD017657.

Zhou, H., G. Diendorfer, R. Thottappillil, H. Pichler, and M. Mair (2011), Mixed mode of charge transfer to ground for initial continuous current pulses in upward lightning, *Proc. 7th Asia-Pacific Int. Conf. on Light. (APL)*, 677–681, doi:10.1109/APL.2011.6110212.